



OPEN Dissolved load, chemical weathering, and CO₂ uptake dynamics of small tropical mountainous rivers of Southern Granulite Terrain, Karamana and Vamanpuram, Western Ghats, India

B. Upendra^{1,2}✉, M. Ciba¹, S. Rahul¹, G. Sreenivasulu¹, S. Kiran Kumar Reddy³, V. Arun¹ & K. Anoop Krishnan¹

Chemical weathering in a river basin is a key geochemical process that controls fluxes between the atmosphere, land, and ocean, playing a crucial role in regulating Earth's climate, particularly the small tropical mountainous rivers with high weathering yield. This study delves into the dissolved solute chemistry of two small tropical mountainous rivers in India's Southern Granulite Terrain (SGT): the Karamana River Basin (KRB) and Vamanapuram River Basin (VRB), together referred as KVRB. Seventy-two water samples (36 per river) that are collected across three seasons are analysed for various physio-chemical parameters using standard methods. A chemical mass balance (CMB) model was employed to quantify solute sources, while silicate weathering rates (SWR), and CO₂ consumption rates (CCR) were estimated separately. Results show that silicate weathering is the dominant process, followed by anthropogenic and atmospheric contributions, particularly at the river outlets. At the KRB outlet, SWR is 30.96 t km⁻² yr⁻¹, and CCR is 1.16 × 10⁶ mol km⁻² yr⁻¹, whereas VRB shows lesser values of 22.89 t km⁻² yr⁻¹ and 3.20 × 10⁵ mol km⁻² yr⁻¹. The lower Arrhenius activation energies of 27 kJ mol⁻¹ for KRB and 25 kJ mol⁻¹ for VRB are evident for intense silicate weathering. Additionally, the physical weathering rates (PWR), evaluated using total suspended solids (TSS) concentrations, are more significant in KRB, particularly during the monsoon, due to its steep terrain and humid climate; while VRB experiences less physical weathering. The study emphasizes the complex interaction of silicate and physical weathering processes with climate and geomorphological conditions of KVRB.

Keywords Hydrogeochemistry, Tropical mountainous rivers, Karamana river basin, Dissolved solute controlling factors, Silicate weathering, CO₂ consumption, Southern Granulite Terrain

River basins are critical biogeochemical interfaces for natural resources like rock, water, air, organic matter, and soils, which support habitats and essential resources^{1,2}. The chemistry of dissolved solutes connects the continental-ocean-atmosphere system through various processes^{3,4}. Continental weathering primarily produces dissolved solutes, with erosion aiding in their distribution across the geosphere, thus supporting essential elements for geosphere-dwelling species^{5–10}. The interaction of water, atmospheric CO₂, and rocks leads to the dissolution of soluble salts from rock minerals, where the dissolution of CO₂ in water, releasing the protons helps in dissolving these minerals. Chemical weathering of silicate rocks plays a key role in long-term climate change, as weathering removes CO₂ from the atmosphere and stores it in sediments. Silicate rock weathering,

¹Biogeochemistry Group, National Centre for Earth Science Studies (NCESS), Thiruvananthapuram 695011, India.

²Department of Applied Chemistry, Cochin University of Science and Technology (CUSAT), Kochi 682022, India.

³Centre for Marine Living Resources & Ecology, Kochi 682508, India. ✉email: upendra.ncess@gmail.com

which covers 83% of land surfaces, is significant for CO₂ consumption and climate regulation, despite carbonate weathering being faster^{11–13}. Understanding the driving factors and feedback loops that influence Silicate Chemical Weathering Rates (SWR) and the associated Carbon Dioxide Consumption Rate (CCR) is a significant challenge and are needed to be estimated for the long-term global carbon cycle budget modelling. Factors influencing silicate weathering rates include basin runoff, lithology, temperature, vegetation, and relief^{14–16}. Numerous research on dissolved solute loads has explored their sources and controlling mechanisms^{17–33}. Studies on chemical weathering and CO₂ consumption in rivers such as the Amazon, Congo, Niger, Mekong, Pearl, Yellow, and Yangtze have provided substantial insights^{5,24,34–43}. In India, relevant studies have examined dissolved solute loads and weathering^{44–51,109}, with a focus on silicate weathering, CO₂ consumption, and solute quantification^{3,4,15,16,20,52–54,68}.

Milliman & Farnsworth⁵⁵ noted that small tropical mountainous rivers contribute more dissolved flux to the ocean compared to larger rivers, for example the mean global sediment and dissolved solids yield of small tropical mountainous rivers are 870 t/km²/yr and 110 t/km²/yr are much higher compared to corresponding attributes of 115 t/km²/yr and 30 t/km²/yr of the global rivers even though the small tropical rivers drains through only 10% while the global rivers drains through 90% of the continent highlighting the need to understand the solute acquisition pathways as well as the source-wise solute load quantification from these rivers along with the respective SWR and associated CO₂ draw down rates. The Western Ghats (WGs) rivers in southern India, characterized by high runoff, average elevation ~ 1200 m, mean rainfall ~ 3550 mm, and a humid tropical climate, are typical for the small tropical mountainous rivers dominated by silicate basement, Southern Granulite Terrain, and Dhrwar Craton. These rivers play a vital role in marine ecosystems, Western Ghats biodiversity and are facing the water-related challenges due to population density, rapid socio-economic development and industrial activities^{55–58}. Understanding the role of these rivers in regional geochemical cycling and climate regulation is essential, especially given the limited data on natural and anthropogenic impacts on water quality. Prior studies have addressed dissolved solute load flux^{56,59–61} and weathering rates and CO₂ consumption^{14,26,62–64}.

This study focuses on the Karamana (KRB) and Vamanapuram (VRB) river basins (KVRB), two small tropical mountainous rivers in the southern Western Ghats, to investigate solute sources, controlling factors addressing a significant knowledge gap in understanding the solute dynamics of small tropical rivers. By analyzing solute sources, acquisition mechanisms, and quantification of solute loads. It emphasizes anthropogenic activities, chemical weathering, and CO₂ consumption rates to establish a baseline dataset of hydro-geochemical parameters for monitoring future environmental changes. These findings offer critical insights into the global significance of small tropical mountainous rivers, particularly in the context of chemical weathering, CO₂ drawdown and source-wise solute load quantification and contribute to the broader understanding of riverine influences on oceanic and atmospheric systems.

Study area

The study area encompasses two small tropical mountainous river basins, the Karamana River Basin (KRB) and the Vamanapuram River Basin (VRB), both situated in the southern part of India. These basins collectively cover a significant portion of the Thiruvananthapuram district. The KRB spans approximately 606 square kilometers, while the VRB covers around 702 square kilometers, together encompassing an area of nearly 1308 square kilometers based on the digitized hydrologic base data from Bhuvan 2D. In the present study, we are focusing solely on the region up to Thiruvallam for KRB and excluding the Parvathy Puthanar's confluence with the river beyond the Thiruvallam. This is because the area beyond Thiruvallam is influenced by saline water intrusion, and Parvathy Puthanar is an artificial canal along the coast that is connected to the KRB beyond the outlet (Fig. 1). Both basins feature diverse terrain, ranging from coastal plains to the elevated hills of the Western Ghats, with elevations reaching up to 1860 m above sea level. The Karamana River originates from the Chemmunji Mottai hills and flows through the Peppara Wildlife Sanctuary before reaching the Arabian Sea. Similarly, the Vamanapuram River originates from the Chemmunji Mottai hills, with its tributaries, including the Keezhattur Ar, Thodikkakkuzhi Ar, and Mamom Ar, contributing to its flow. The KRB features two dams despite its short length: the Peppara Dam, which is primarily for irrigation in the upper reaches, and the Aruvikkara Dam, serving both irrigation and as a drinking water supply for the city of Trivandrum (Fig. 1). On the river's western side, water flow is impeded by significant silting at Munnattumukku and sea sand accumulation at Kunnumanal. During high tide, seawater from the estuary can travel up to Thiruvallam via the eastern side of Edayar. When the tide recedes, polluted water from the Parvathy Puthanar flows upstream, affecting areas up to and beyond Thiruvallam.

The region is a chunk of Southern granulite terrain (SGT) and hence the major rocks of the region are crystalline rocks of Archean age and metasediments named leptynites (garnet-biotite gneiss), khondalite (garnet-biotite-sillimanite gneiss + graphite) gneiss of Proterozoic age with some pegmatite veins, dolerite dykes, and quartz veins. However, the coastal stretch of the region comprised quaternary sediments and warkalli beds distinguished as disconnected patches on crystalline¹⁰⁷. The climatic conditions of these basins are characterized by a tropical monsoon climate with distinct seasons: pre-monsoon (March to May), SW monsoon (June to September), NE monsoon (October to December), and a postmonsoon (January to February)⁶¹. This distinctive climatic character of KVRB is attributed to the Western Ghats barrier, which keeps eastern and western climatic diversity separate, as the western portion receives more rainfall and has a humid climate rather than the arid climate in the eastern part of southern India⁶¹. The long-term annual average rainfall spatially varies between 2500 mm and 3500 mm, influenced by the orographic features of the Western Ghats for example, for the 2020 year the annual rainfall is ~ 2520 mm (Figure S1). The mean temperature of the region, determined from atmospheric data gathered at multiple sampling locations during the study is approximately 30°C (Table S1).

Land use in these basins is a mix of agriculture, forests, plantations, and urban areas. The vegetation includes tropical evergreen and semi-evergreen forests in the higher elevations, along with rubber and tea plantations

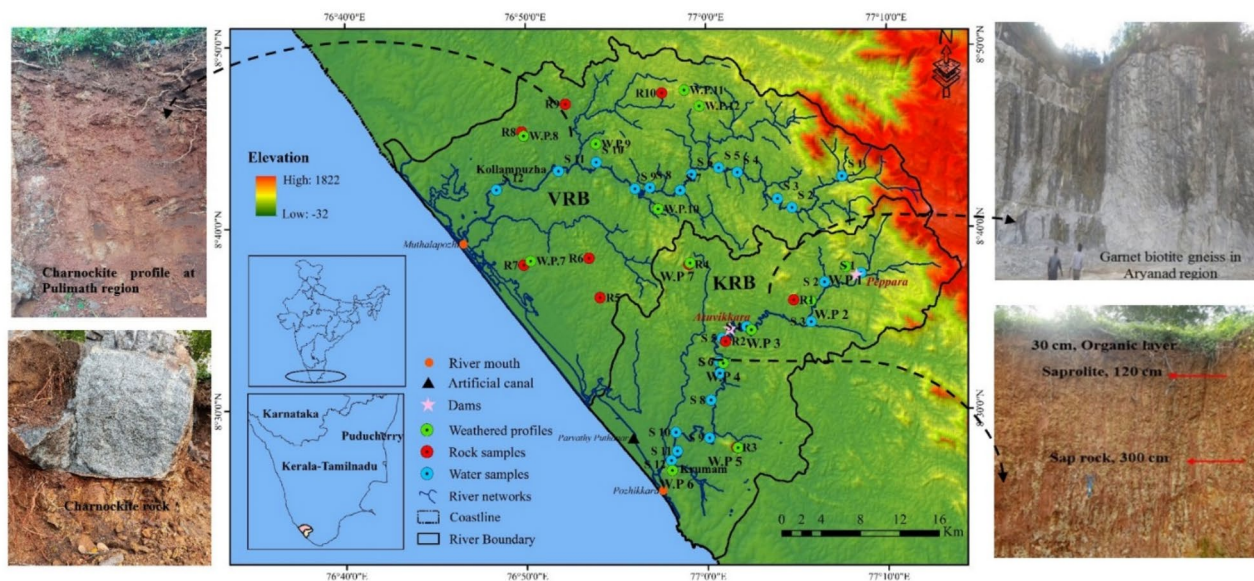


Fig. 1. Map showing the Karamana and Vamanapuram river basins and their tributaries in southwestern India. The map was created using the Bhuvan 2D platform and refined using ArcGIS software (version 10.7). The background includes the Digital Elevation Model (DEM) of the watershed, with locations of water, rock, and weathered profile sampling, along with dams and artificial canals. DEM data were obtained from the Shuttle Radar Topography Mission (SRTM) database (<https://dwtkns.com/srtm30m/>) and processed with ArcGIS (<https://resources.arcgis.com/en/help/main/10.7/>).

and paddy fields in the plains^{65,66}. The primary soil types identified in the KVRB region, according to the FAO (Food and Agricultural organization of United Nations), are Nd48-2-3b-3817, Ap21-2b-3656, Rd23-1a-3844, and Nd47-2b-3816. Texturally, these soils are classified as sandy clay loam, clay loam, sandy loam, and gravelly clay. The socio-economic activities in the region are primarily agricultural, with crops such as rice, coconut, rubber, and spices being predominant. Additionally, eco-tourism is gaining importance, particularly in areas like the Kallar eco-tourism region, which is noted for its well-preserved environment⁶⁵⁻⁶⁷. Environmental concerns in the KRB and VRB include water pollution from agricultural runoff, untreated sewage, industrial effluents, deforestation, and soil erosion⁶⁷. Flooding during the monsoon season is also common, affecting farming lands and settlements. Therefore, a river basin study is adequate to promote the preservation of natural habitats and sustainable resource management of the two chosen river basins, KRB and VRB, together named KVRB.

Materials and methods

Sampling

In the present study, geo-environmental samples, namely water, soil, weathered profile, and rock representing the different geo-environmental species are collected within the region. Here, the rock, weathered profile, and topsoil are considered as aseasonal as they remain unaffected by climate dynamics on yearly scale. Initially, water samples from the KVRB are collected and analyzed using the standard analytical procedures that generate hydrochemical data of major anions and cations utilized in the present study. A total of 72 water samples were collected from 12 different locations along the mainstream of each river, with 32 samples from each river. Sampling sites were strategically selected based on geological, land use, and topographical variations, as well as the potential impact of coastal saline water intrusion. For precise data collection, mouth samples are collected 1 km upstream from where the river meets the ocean. The sampling locations were deliberately selected downstream of tributary confluences to ensure their influence was accounted for in the calculations. The samples were gathered during three distinct seasons: pre-monsoon (March), monsoon (September), and post-monsoon (January) over the years 2019–2022, this temporal frequency has been followed because the study area is dominated by high rainfall in the monsoon season. The seasonal samples are labeled as KRB-PRM, KRB-MON, and KRB-POM for the KRB, and VRB-PRM, VRB-MON, and VRB-POM for the VRB, corresponding to pre-monsoon, monsoon, and post-monsoon periods, respectively. Water samples were collected in pre-washed and labeled 1-liter and 500-milliliter polyethylene bottles for anion and cation analysis, respectively. To preserve metal cations, 1–2 drops of 2 N HNO₃ were added to the 500-milliliter samples immediately after collection. Discharge of the river at the mouth of Maruthoorkadavu (KRB S12) and Poovanpara (VRB S12) are measured seasonally during the collection of water samples and are given in the Supplementary Table. S2.

Topsoil samples were gathered in zip-lock polyethylene bags from areas adjacent to the river course to evaluate their impact on water chemistry (Fig. 1). During collection, each shovel was cleaned with distilled water and thoroughly dried to prevent dust contamination. The rock samples were obtained from freshly exposed rocks in quarry regions, as shown in Fig. 1. Collection was guided by a base map from the Geological Survey of

India (GSI), ensuring samples from each lithology were taken from the north, south, east, and west directions along the river course. Due to variability in rock exposure, samples were collected from the most accessible fresh rock exposures at different quarry locations. Lithologies such as Leptynites, Khondalite, Biotite Gneiss, and Charnockites were collected from various directions along the river. The weathered profiles were sampled near quarry locations wherever available (Fig. 1). These profiles were carefully collected to avoid disturbing the overlying soil and to minimize contamination. Field identification of weathered profiles was based on visual inspection of color, texture, and weathering characteristics. Samples were labeled according to their location, depth, and material properties, as detailed in Fig. 1. The region's weathered profiles are primarily covered by laterite soil, with variations in color, texture, and appearance depending on the underlying lithology. All the collected water, rock, soil, and weathered profile samples were sent for further laboratory analysis.

Data generation and validation

The collected water, soil, channel sediments, rock, and weathered profiles samples, are subjected to geochemical analysis in the laboratory using various analytical instruments. The in-situ measurements like pH, TDS, EC, and temperature (both atmosphere and water temperature) are taken in the field using water SONDE (OTT HydroMet, DS 5X model). Subsequently, water samples are carefully transported to the laboratory for thorough chemical analysis. Before conducting the chemical analysis of water samples, a portion of the sample is filtered using filter paper to examine the total suspended sediments (TSS). The filtration process is performed using Whatman No. 42 filter paper, and the sediment retained on the filter is weighed after drying to determine the TSS. Cations are examined using the Microwave Plasma Atomic Emission Spectroscopy (MP-AES) instrument (Agilent, 4210 model), while anions are assessed through the Dionex™ Ion Chromatography (ThermoFisher, 4210 model). Bicarbonate levels are determined utilizing the Alkalinity test kit from Metrohm, and the detection of silica (SiO₂) is achieved using the Continuous Flow Analyzer (CFA) device (Skalar, San ++ model). The obtained hydrochemical data of water samples are then validated using a normalized inorganic charge balance ion (NICB) test using the following Eq.

$$\text{NICB} = \left[\frac{(\text{Tz}^+ - \text{Tz}^-)}{(\text{Tz}^+ + \text{Tz}^-)} \right] \times 100 \quad (1)$$

The NICB (in %) expresses the magnitude of the deviation between the sum of cations charge (Tz⁺) and the sum of anions charge (Tz⁻) in equivalents⁶⁸. There is an overall balance of major ions in all 72 sample data points (Table 1), indicating that NICB values are generally within 10%. The NICB corrected values are further used for studying the hydrochemical nature of the basin.

Considering the KVRB flows through the rugged terrain of the Western Ghats and the coastal regions of Kerala, evaluating the suspended load chemistry is crucial^{69,70}. Sample analyses have revealed dark-stained filter papers, particularly at downstream sites, indicating heightened physical weathering processes within the basin. To better understand these processes, the total suspended load (TSS) is estimated using the following equation.

$$\text{TSS} = (M_1 - M_0) * 1000000 / V_0$$

In this context, M₀ and M₁ indicate the filter's weight in milligrams before and after the filtration process, respectively, while V₀ refers to the volume of the sample taken for filtration, measured in liters.

The collected weathered profile samples and soil samples were washed and dried in an oven at 60°C and then 5 g of the dried samples were taken by the coning and quartering method. The 5 g samples are powdered using an agate mortar up to a size less than 74 micron (ASTM 200 mesh). All these powdered samples are taken for XRF analysis to get elemental geochemical composition. Before XRF analysis, the loss of ignition (LOI) of samples is measured using the Muffle furnace in which the samples are ignited up to 900°C. The Loss of ignition of samples is estimated in percentage (%) and is calculated using Eq. (2)

$$\% \text{ of loss of ignition} = \frac{W_2 - W_1}{W_2} \times 100$$

In the above equation, W₂ is the weight of sample in mg before ignition, W₁ - weight of sample in mg after ignition. In the same way, weathered profile samples and soil samples are analysed in which the weather profiles from each depth have been measured separately. However, the rock samples that are consolidated in nature are also performed with the geochemical investigation in which hard rock samples are first washed, braked to small pieces and powdered using TEMA mill, which are subjected to XRF analysis. Like the other unconsolidated samples, LOI of the powdered rock samples are taken before analysis.

Data interpretation

Further, the identification and characterization of the processes that control dissolved load solute are depicted through diverse graphical plots including Gibbs diagram, bivariate scatter plot of elemental/ionic ratios, and mixing diagram.

Dissolved load source characterization – Gibbs, bivariate plots

The dissolved solute controlling process of KVRB is recognized by portraying Gibb's (1970) diagram, bivariate plot of elemental species. Further, a Na-normalized mixing diagram is fabricated to assess the weathering character of the basin. Consequently, the contribution of sources to a dissolved load of KVRB is quantified using the mass balance model. The methodology employed for constructing mixing diagrams and estimating quantification is described in detail below.

Weathering mechanism of basin: mixing diagram

To examine the weathering mechanism in the basin, the study adopts the Na-normalized Ca versus Mg mixing analysis proposed by Gaillardet et al.²⁴, which depicts three end-members namely Evaporites, Silicates, and Carbonates of primary rocks. Many hydrochemical researchers^{9,13,26} have used the aforementioned diagram for evaluating the weathering contribution from different source rocks. Nevertheless, the study by Upendra et al.⁶⁸ modified the mixing diagram by accounting for the Na-normalized Ca versus Mg ratios of secondary minerals in the soil and weathered profile in addition to the three primary end-members proposed by Gaillardet et al.²⁴. The secondary mineral end-member in the study represent the silicate minerals present in the topsoil as well as in the weathered profile that are developed over dominant lithology. The same criteria are adopted in the current study by constructing a Na-normalized mixing diagram constituting 4 end-members namely; rock end members, soil with a weathered profile, carbonates, and evaporites. To construct the mixing diagram for KVRB, first, the mixing diagram proposed by Gaillardet et al.²⁴ is plotted with evaporites, silicates, and carbonate end-members. Then the Na-normalized Ca versus Mg elemental ratios are calculated for the lithological, soil, and weathered profile samples of KVRB and are incorporated into the existing mixing diagram proposed by Upendra et al.⁶⁸. The plotted ratio of lithological elemental concentration of each lithology and their average values represents the rock end-member of KVRB while the soil with weathered profiles is the average of all Ca and Mg values (Na-normalized) accommodating silicate minerals present in the soil as well as in the weathered profile developed over various lithologies. The elemental concentration of the lithological, soil, and weathered profile samples are estimated from the oxide weight% of elements obtained through XRF analysis as mentioned in "sampling" Sect. This weight% value of elemental oxide is converted to elemental molar concentration using geochemical conversion. The two end-members namely, rock end-member, and soil with a weathered profile, are added to the pre-existing end-members diagram by Gaillardet et al.²⁴. Thus, the Na-normalized end-member mixing diagram constituting 4 end members of KVRB is developed.

Quantification of source-wise input to the dissolved load: mass balance model

The chemical mass balance forward model is used to quantify the dissolved solutes in river waters of KVRB^{8,40,52}. According to the model, the chemical mass budget of any solute 'X' in river can be written as:

$$X_{rw} = X_{atm} + X_{anthro} + X_{chem.weath} ; \text{ such that } X_{chem.weath} = X_{sil} + X_{carb} \quad (2)$$

where, X is the concentration of solutes, and the subscript rw, atm, anthro, and chem.weath represent the river water, atmospheric, anthropogenic and chemical weathering, while the sil and carb represents the silicate and carbonate minerals respectively.

Atmospheric input

According to Ding et al.⁷¹, correcting the atmospheric contribution is the primary step in the studies regarding the contribution of dissolved load to the river water. In current study, the atmospheric contribution of KVRB estimated using the Cl as proxy due to its conservative nature within the basin as suggested by various researchers⁷¹⁻⁷⁵. Thus, the equation used to correct atmospheric input to rivers for any given element 'X', can be written as^{68,74,76}:

$$X_{atm} = (X/Cl)_{rain} \times Cl_{ref} \quad (3)$$

In the Eq. (2), the X_{atm} corresponds to the molar concentration of any element (Na, K, Ca, Mg etc.) from atmospheric deposition; the $(X/Cl)_{rain}$ is the molar ratio of any element to the Cl in rain (Table 2) while Cl_{ref} is the critical Cl concentration. Here, the critical Cl concentration represents the product of Cl from rain (Cl_{rain}), evapotranspiration (F_{et}), atmospheric wet and dry deposition ($F_{deposition}$) processes (i.e., $Cl_{ref} = Cl_{rain} \times F_{et} \times F_{deposition}$). The Cl_{ref} used for the study represents the maximum atmospheric input to the river from the precipitation process (wet, throughfall, dry deposition, and evapotranspiration) as the rainwater concentration is not alone sufficient to account for the atmospheric processes^{68,77,108}. In the current study, the Cl_{river} of the upstream is taken as Cl_{ref} as the samples S1 (KRB1, VRB1) of KVRB is collected from the dams, which encompasses all the components of Cl_{rain} , F_{et} , and $F_{deposition}$.

Anthropogenic contribution

In the study area, there are no other sources of Cl besides the atmosphere and anthropogenic sources (Fig. 1). As a result, we quantify the anthropogenic contribution to KVRB solute load based on Cl_{ref} in relation to the following two facts: 1) when the measured concentration of Cl in KVRB is lower than Cl_{ref} the entirety of chloride in the river water is attributed to an atmospheric origin; and 1) if it surpasses Cl_{ref} the residual chloride (Cl_{res}) in river water, after atmospheric correction, is attributed to anthropogenic input^{68,74}. In KVRB, Cl_{ref} estimated is less than the measured concentration, the remaining Cl after atmospheric correction is applied to anthropogenic input based on the following mathematical expression.

$$Cl_{res} = Cl_{anthro} = Cl_{river} - Cl_{ref} \quad (4)$$

Moreover, the study also assumes that the Na contribution from the anthropogenic source is equal to the Cl from the anthropogenic source.

$$Na_{anthro} = Cl_{anthro} \quad (5)$$

Sample name	pH	Temperature (°C)			TDS mg/L			TSS mg/L			Na mg/L			K mg/L			Ca mg/L			
		PRE	MON	POM	PRE	MON	POM	PRE	MON	POM	PRE	MON	POM	PRE	MON	POM	PRE	MON	POM	
KRB1	6.69	6.37	5.25	28.5	20.2	28.9	36.86	13.45	13.80	0.69	2.74	1.8	2.00	1.18	1.40	1.10	1.28	1.09	1.24	
KRB2	6.54	6.69	5.31	24.8	21.4	28.5	38.04	17.60	13.54	0.47	5.88	10.9	2.65	1.88	1.65	1.21	1.96	1.32	1.37	
KRB3	6.62	6.58	5.04	24.6	23.2	28.2	38.61	23.83	16.98	9.69	10.75	12.66	3.00	1.94	2.39	1.51	2.15	1.89	1.52	
KRB4	6.51	6.78	5.14	25.9	25	26.5	40.90	26.26	20.84	4.21	16.82	10.02	3.85	1.96	3.31	1.59	2.92	2.01	1.56	
KRB5	6.77	6.68	5.18	26.4	26	29.3	43.57	31.72	21.42	6.61	24.43	12.38	4.58	1.99	3.74	1.74	3.98	2.82	2.23	
KRB6	6.75	6.71	5.21	26.5	26	28.4	45.00	36.93	23.65	13.18	23.71	16.94	5.26	2.02	4.35	1.85	4.11	3.09	2.26	
KRB7	6.82	6.67	5.31	25.9	25.5	28.8	47.43	38.75	23.76	11.97	47.86	14.12	5.47	2.53	4.49	1.88	4.32	3.23	2.30	
KRB8	7	6.83	5.44	26.5	26	27.9	50.00	43.34	26.76	15.28	61.13	17.78	5.68	2.65	3.70	1.87	4.50	4.09	2.60	
KRB9	6.97	7.15	5.49	26.3	26.1	27.4	55.00	48.91	33.17	15.42	61.68	23.18	6.54	2.82	4.50	2.10	4.75	4.27	2.74	
KRB10	6.72	6.51	5.62	26	26	27.7	61.29	53.78	34.86	6.27	25.09	14.04	6.99	2.99	4.68	2.12	4.97	4.63	2.89	
KRB11	7.02	6.95	5.68	27.5	26.5	27.8	60.71	56.65	36.66	7.90	31.58	14.6	7.57	3.08	5.19	2.16	5.05	4.84	3.31	
KRB12	6.79	6.97	5.74	27.1	26.1	27.8	67.14	60.60	38.01	8.53	34.12	12.7	9.63	3.17	5.74	2.18	5.94	5.33	3.91	
VRB1	7.22	7.36	7.72	27.5	25.8	21.5	27.67	13.09	18.12	5.9	2.39	8.1	1.80	1.01	1.35	0.85	1.24	1.05	1.25	
VRB2	7.05	7.32	7.72	29.5	27.7	25	25.87	16.37	21.34	4	4.64	8.3	2.38	1.32	1.76	1.34	1.72	1.26	1.41	
VRB3	7.06	7.3	7.7	31.5	27.3	25.5	25.83	17.14	23.18	7.1	6.40	3.2	2.46	1.36	1.86	1.32	1.85	1.38	1.60	
VRB4	6.6	7.25	7.32	28.5	27.8	26	26.61	19.06	24.46	6.3	14.80	5.1	2.54	1.49	1.89	1.51	2.15	1.46	1.79	
VRB5	6.64	7.21	7.23	30.5	27.7	25	24.39	21.30	25.05	6.3	7.96	3.3	2.86	1.47	2.05	1.55	2.19	1.59	1.84	
VRB6	6.99	7.23	7.77	27.5	28.2	25	25.08	22.58	26.68	5.5	9.08	3.1	2.97	1.53	2.24	1.61	2.29	1.63	1.94	
VRB7	6.8	7.35	7.79	28.5	28.4	26	25.27	24.65	28.19	11.6	8.76	6.4	3.01	1.49	2.49	1.64	1.97	1.70	1.99	
VRB8	6.98	7.52	7.8	28.5	28.3	28	28.4	25.48	29.34	0.2	11.16	3.2	3.38	1.51	2.67	1.80	2.05	1.89	2.01	
VRB9	7.03	7.49	7.81	28.5	28.5	26	30.84	26.95	29.79	5.1	7.20	3.5	3.45	1.62	2.74	1.96	2.33	1.93	2.29	
VRB10	7.01	7.56	7.87	29.5	28.9	25	36.84	31.28	30.41	5.7	6.60	4.2	4.76	1.88	2.90	2.07	2.86	2.20	2.48	
VRB11	6.99	7.75	7.81	30	28	27	45.84	34.82	39.24	8.9	13.96	3.2	5.26	2.41	3.32	2.26	3.34	2.29	2.64	
VRB12	6.85	7.58	7.68	29.5	28.2	24.5	43.18	42.77	46.35	5.5	16.28	4.3	6.38	2.63	3.98	2.31	3.27	2.91	2.88	
Sample name	Mg mg/L	Cl mg/L			HCO ₃ mg/L			SO ₄ mg/L			NO ₃ mg/L			SiO ₂ mg/L			NICB (%)			
		PRE	MON	POM	PRE	MON	POM	PRE	MON	POM	PRE	MON	POM	PRE	MON	POM	PRE	MON	POM	
KRB1	0.69	0.40	0.47	2.02	1.94	1.84	9.70	3.34	6.53	1.17	0.86	0.16	0.50	0.82	0.56	3.96	3.24	3.34	4.90	5.37
KRB2	0.79	0.61	0.65	3.02	1.97	2.06	10.30	6.73	7.33	1.70	0.28	0.28	1.01	0.82	0.74	4.74	3.51	3.61	5.15	6.99
KRB3	0.95	0.83	0.61	3.54	2.36	2.89	11.20	10.12	7.51	2.09	0.46	0.30	1.85	0.97	0.76	5.16	3.99	4.07	4.83	9.53
KRB4	1.05	0.86	0.66	4.80	2.79	3.87	12.40	10.68	8.00	2.58	0.87	0.50	2.00	1.26	1.07	5.17	4.12	4.32	3.06	8.48
KRB5	1.31	1.08	0.70	6.16	3.85	3.95	13.00	12.11	9.21	2.97	1.59	0.61	2.28	1.46	1.19	5.22	4.23	4.37	7.01	5.08
KRB6	1.33	1.09	0.71	6.77	4.34	4.35	13.80	14.10	9.49	3.03	2.15	0.83	2.07	2.03	1.25	5.48	4.39	4.49	7.51	3.23
KRB7	1.35	1.20	0.71	7.08	4.60	4.38	14.80	15.31	10.41	3.02	2.35	0.84	2.07	1.40	1.31	5.51	4.47	4.57	7.93	4.27
KRB8	1.44	1.49	0.76	7.28	4.86	4.98	14.60	17.90	10.93	3.36	2.59	1.01	2.70	1.27	1.51	5.59	4.58	4.78	8.38	6.50
KRB9	1.56	1.50	0.90	8.55	5.88	6.22	19.60	19.67	11.33	3.44	2.92	1.37	2.43	2.42	1.84	5.74	4.71	4.79	3.64	5.25
KRB10	1.88	1.53	1.00	9.23	5.91	6.47	21.20	22.74	11.92	3.37	3.21	1.61	2.27	2.63	1.95	6.24	5.17	5.27	4.76	4.59
KRB11	2.07	1.56	1.07	9.51	7.26	7.05	22.40	23.16	13.30	3.34	3.24	1.88	2.07	2.55	1.97	6.32	5.19	5.29	6.05	4.66
KRB12	2.39	1.82	1.09	12.57	7.82	7.56	23.40	24.97	15.56	3.57	3.34	1.96	2.19	2.52	1.99	6.28	5.43	5.63	8.08	4.52

Continued

Sample name	Mg mg/L			Cl mg/L			HCO ₃ mg/L			SO ₄ mg/L			NO ₃ mg/L			SiO ₂ mg/L			NICB (%)		
	PRE	MON	POM	PRE	MON	POM	PRE	MON	POM	PRE	MON	POM	PRE	MON	POM	PRE	MON	POM	PRE	MON	POM
	VRB 1	0.74	0.40	0.69	1.29	0.89	1.14	4.68	4.03	4.59	1.16	0.81	1.12	0.28	0.13	0.16	5.76	3.58	5.06	-1.93	-5.56
VRB 2	1.07	0.43	0.75	1.97	0.98	1.46	7.03	4.86	5.48	1.20	0.82	1.14	0.29	0.16	0.19	6.62	4.01	5.79	0.51	1.63	-2.07
VRB 3	1.12	0.55	0.78	2.09	1.05	1.56	7.61	5.05	6.65	1.25	0.88	1.16	0.34	0.22	0.27	7.02	4.09	5.62	-0.53	3.87	-2.87
VRB 4	1.16	0.63	0.81	2.42	1.11	1.63	7.73	5.95	7.27	1.35	0.90	1.23	0.68	0.59	0.62	5.85	3.99	6.32	3.36	2.50	-4.92
VRB 5	1.45	0.84	0.76	2.80	1.14	2.06	9.96	6.90	8.13	1.36	0.86	1.33	0.73	0.63	0.58	4.55	4.14	5.45	4.71	6.53	-5.77
VRB 6	1.54	0.91	0.76	2.92	1.24	2.53	10.83	7.51	8.87	1.38	0.86	1.16	0.74	0.79	0.80	4.93	4.23	5.43	3.70	5.37	-6.96
VRB 7	1.18	1.11	0.75	3.27	2.45	2.72	9.37	8.28	9.39	1.50	0.89	1.36	0.75	0.90	0.64	5.44	4.58	6.09	-1.70	0.89	-8.48
VRB 8	2.04	1.13	0.85	3.29	2.51	3.25	12.47	8.59	9.62	1.32	1.16	1.40	0.74	0.93	0.66	7.14	4.19	6.26	0.43	4.00	-8.06
VRB 9	2.11	1.15	0.91	3.36	2.64	3.38	14.05	9.36	11.93	1.34	1.14	1.42	0.85	0.97	0.84	7.38	4.32	5.72	-0.43	2.96	-8.75
VRB 10	2.23	1.24	1.03	4.09	3.55	3.50	14.93	11.89	13.15	1.58	1.47	1.44	0.89	0.97	0.82	7.23	4.55	6.19	5.14	-0.28	-8.37
VRB 11	2.35	1.44	1.19	5.12	5.96	3.96	15.52	13.34	14.96	1.98	1.61	1.80	0.98	0.98	0.92	7.94	4.46	6.65	5.39	0.37	-9.02
VRB 12	2.66	1.63	1.24	6.29	6.10	5.05	20.58	16.64	15.69	2.55	2.17	2.31	0.99	1.03	0.93	6.93	4.47	6.36	2.22	1.88	-8.45

Table 1. Hydrochemical data of KVRB with NICB values for the three seasons; Pre-monsoon (PRE), monsoon (MON), and Post-monsoons (POM).

Basin	Na _{rain} (umol/L)	K (umol/L)	Ca (umol/L)	Mg (umol/L)	Cl (umol/L)	SO4 (umol/L)	NO3 (umol/L)
KVRB	46	4	19	10	43	9	2

Table 2. Rain water composition collected for KVRB.

Additionally, there are remaining SO₄ and NO₃ presence observed for KVRB in the midstream to downstream regions after the atmospheric correction and are also considered to be delivered from the anthropogenic input with the facts. These ions are together balanced with Ca and Mg equally the fact they came from a similar source such as a sewage pipeline which is a common problem in the KVRB as mentioned by many studies⁷⁸. Anthropogenic influences have become more significant in the KVRB in recent years, particularly due to rapid socio-economic development in the region^{65,78}. The primary anthropogenic sources in the KVRB include agricultural runoff, industrial discharges, urbanization, and waste disposal⁷⁸. The use of fertilizers and pesticides in agriculture contributes to nutrient pollution, while urbanization leads to increased sewage and wastewater contamination. Industrial activities further release pollutants into the rivers, negatively affecting both the ecosystem and public health. However, due to the interconnected nature of these factors, it is not possible to separate the individual effects of each anthropogenic contributor, which is a limitation of this study. The impact is more significant in the KRB than in the VRB because it is situated in a densely populated area, with cities like Thiruvananthapuram nearby, as outlined in Sect. 2 of the study.

Chemical weathering input

Proxies like atmospheric input corrected Na (Na^{*}), atmospheric and anthropogenic input corrected Na (Na_{sil}), or atmospheric input corrected Mg (Mg^{*}) concentrations in river waters can serve as tools to estimate the solute load in the KVRB resulting from the chemical weathering of silicate rocks^{8,26,52,79}. According to the bivariate plots, Gibbs diagram, and chemical weathering diagram, the Na in the KVRB is derived from different sources such as silicate weathering, anthropogenic activities, and atmospheric input. Considering the absence of carbonate rocks (Fig. 1) in the river basin, these rocks are not included in the estimation of chemical weathering contribution. Like previous studies⁷⁵, the Na contribution of silicate weathering is calculated after correcting river water concentrations of Na (Na_{rw}) from anthropogenic (Na_{anthro}) and atmospheric (Na_{atm}) inputs via the Cl_{ref} using Eq. (8). To compute the K input from silicate weathering within the KVRB, it is further assumed that the entire K in river waters originates from silicate weathering and atmospheric intake following the study by Upendra et al.⁶⁸. Hence, after accounting for atmospheric input, residual K in river waters is attributed into silicate weathering. Further, two general assumptions are used to estimate the silicate weathering contributions of Ca and Mg using the Na_{sil} silicate component as a proxy^{7,26}. The assumptions are (1) the Ca_{sil} and Mg_{sil} released into the river water relative to the Na_{sil} in a fixed proportion, and (2) the anthropogenic Ca and Mg contributions are equal in proportions. Thus, the contribution from silicate weathering can be expressed by the following budget equations;

$$\text{Na}_{\text{sil}} = \text{Na}_{\text{rw}} - \text{Na}_{\text{atm}} - \text{Na}_{\text{anthro}} \quad (6)$$

$$\text{K}_{\text{sil}} = \text{K}_{\text{rw}} - \text{K}_{\text{atm}} \quad (7)$$

$$\text{Ca}_{\text{sil}} = \text{Na}_{\text{sil}} \times (\text{Ca}/\text{Na})_{\text{rock}} \quad (8)$$

$$\text{Ca}_{\text{sil}} = \text{Na}_{\text{sil}} \times (\text{Ca}/\text{Na})_{\text{rock}} \quad (9)$$

$$\text{Mg}_{\text{sil}} = \text{Na}_{\text{sil}} \times (\text{Mg}/\text{Na})_{\text{rock}} \quad (10)$$

where the subscripts rw, sil, anthro, and atm refer to river water, silicate, anthropogenic, and atmosphere input respectively; while the (Ca/Na)_{rock} and (Mg/Na)_{rock} are the Ca and Mg ratios discharged into river waters relative to Na from silicates. In the current study, the values of (Ca/Na)_{rock} and (Mg/Na)_{rock} are taken in the range 0.42–1.16 and 0.35–0.9 respectively for different upstream and downstream stations of KVRB according to the geological composition in the corresponding sample location, based on the average rock composition.

Chemical weathering rates (CWR)

It is necessary to evince the significance of the region by estimating the rates of silicate weathering and CO₂ consumption due to the fact that the dissolved load have significant effect in regulating earth's climate. Since the estimation of weathering rates and CO₂ consumption rates have significant role in relating the dissolved chemistry to climatic scenario, the weathering rates of KVRB is estimated along with CO₂ consumption in the following section.

Approximation of silicate weathering rates (SWR)

To estimate the weathering rates of the KVRB, the study uses the Eq. (9) by considering the fact that there is no carbonate weathering in the basin. Moreover, the estimation of weathering rates at different location are not possible because of the difficulty in measuring discharge data at each location as the KVRB is highly sloped region and the downward erosion is higher in the region causing error in the depth measurement of the basin. Therefore, the estimation is performed exclusively at the downstream regions of KRB and VRB, specifically Maruthoorkadavu (KRB-12) and Ayilam (near VRB-12). This approach is based on the understanding that these locations represent the river's mouth, where the river flux is discharged into the ocean, providing a comprehensive

representation of the river load. There are many methods to evaluate the silicates weathering rates but the study uses the dissolved solute chemical data and discharge (Q) of the KRB as follows:

$$\text{SWR} = (Q/A) \times [(\text{Na} + \text{K} + \text{Ca} + \text{Mg})_{\text{sil}} + \text{SiO}_2] \quad (11)$$

Here, Q is the discharge of the river in m³/sec, A is basin area in km², and rest of the Na, K, Ca, Mg and SiO₂ are the silicate weathering derived dissolved constituents (mg/L) in the river water. The estimated SWR is expressed in t km⁻² yr⁻¹ by using appropriate conversion parameters.

Approximation of CO₂ consumption rates

Several researchers connected continental weathering with atmospheric CO₂ and suggested different models for biogeochemical cycling conveying the link between atmosphere and continental weathering^{22,80–84}. Moreover, the continental weathering dependency on climate has been always looked at within time frame⁸⁴. Since the study area, KVRB is situated in the humid tropical region and drains through a few kilometers of the urban sector, and the fact that silicate-weathering controls the river chemistry it is obvious that the river must have a significant role in regulating the climate of the region. Moreover, the study by West et al.⁸⁵, mentioned that CO₂ consumption by silicate weathering has a significant role in ongoing climatic variation. Hence, the CO₂ consumption by silicate weathering is estimated using Eq. (12) as follows and is expressed by the unit mole km⁻² yr⁻¹.

$$\text{CCR} = (Q/A) \cdot (\text{Na} + \text{K} + \text{Mg} + \text{Ca})_{\text{sil}} \quad (12)$$

Here, the Q is discharge of KVRB in m³/sec, A represent basin area in km², and the Na, K, Ca, Mg and SiO₂ are dissolved constituents (mg/L) in the river water contributed by silicate weathering.

Results and discussion

Hydrochemistry: dissolved and suspended phases

The concentration of dissolved solutes in KVRB are following the order of HCO₃ > Cl > Na > Ca > K > Mg > SO₄ among which the cation abundance is in the order Na > Ca > K > Mg while the anion abundance is in the order HCO₃ > Cl > SO₄. The seasonal values of all physical and chemical parameters of KVRB are displayed in Table 1 with the NICB values. The TDS of the KRB ranges between 13.45 mg/L and 89.41 mg/L with an average value of 41.72 mg/L while for VRB it ranges between 13.09 mg/L to 53.12 mg/L with a mean value of 32.8 mg/L. Since the KVRB represents the small tropical mountainous rivers, the values are compared with some WGs rivers. It is noted that the mean average of KVRB exceeds that of certain WGs rivers, such as the Manimala River basin (MRB; 25.23 mg/L). However, when compared to the Netravati River (38 mg/L), only the KRB value is higher, while the VRB value is lower. However, the TDS values of KVRB are less than the mean TDS calculated for the rivers, Pambar (151)⁶¹, Muthirapuzha (131)⁸⁶, and Achankovil (54 mg/L)⁵⁹. However, the values of KRB are comparable to the World's largest river Amazon (41.71 mg/L), and other larger rivers such as Orinoco (30.13) and Congo (37 mg/L). The Na, Ca, K, and Mg in KRB vary in the range 1.52–13.91 mg/L, 1.18–7 mg/L,

Rivers	Tds average	Ca	Mg	Na	K	Cl	SO4	HCO3	Si	NO3	Reference
	mg/L										
West flowing											
Manimala	25.23	2.44	0.94	2.28	1.07	8.72	2.65	7.03	8.37	0.88	Padmalal et al. ⁵⁶ (2012)
Pambar	151	9.66	6.78	10.52	1.88	30.71	4.71	71.44	2.10		Thomas et al. ⁶¹ (2015b)
Muthirapuzha	131	10.22	5.18	5.61	2.23	36.28	3.75	51.31	2.70		Thomas et al. ⁸⁶ (2014)
Achankovil	54	2.68	1.19	3.26	0.98	23.04	0.58	13.42	4.27		Prasad & Ramanathan ⁵⁹ (2005)
Netravati	38	2.97	1.29	3.17	0.70	3.23	1.15	18.85	11.72		Gurumurthy et al. ² , (2012)
West-flowing rivers of Deccan volcanic province	82	6.85	3.21	3.95	0.23	3.91	1.15	40.57	21.63		Das et al. ⁷⁹ (2005)
Peninsular											
Narmada	248	25.81	10.86	13.99	1.49	4.33	2.88	167.66	19.77		Gupta et al. ³ (2011)
Bhima	347	27.77	13.34	42.47	1.76	33.23	50.72	151.30	22.83		Das et al. ⁷⁹ (2005)
Krishna (upstream)	112	11.86	4.59	6.37	0.55	6.82	3.55	60.46	16.22		Das et al. ⁷⁹ (2005)
Godavari	214	31.17	10.64	27.42	3.91	25.56	18.06	137.39	26.32		Jha et al. ¹⁴ (2009)
Tapti	474	20.32	19.83	69.14	5.32	43.58	17.42	202.4		2.23	Sharma & Subramanian ⁹⁸ (2008)
Himalayan											
Kali River	118.68	11.95	3.23	13.15	1.88	14.48	9.39	53.44	10.81	0.39	Arun et al. ⁶⁴ (2022)
World rivers											
Amazon	41.71	5.58	0.91	2.04	0.90	1.63	2.42	20.38	7.85		Mortatti & Probst ⁸⁷ (2003)
Orinoco	30.13	3.26	0.77	1.34	0.79	0.8	2.78	11.26	7.44	0.03	Laraque et al. ⁸⁸ (2013)
Loire		0.71		0.32		0.67	2.21			1.61	Gaillardet et al. ²⁴ (1999)

Table 3. Hydrogeochemical data of Indian and World's rivers.

0.92–3.73 mg/L, and 0.56–2.91 mg/L, respectively, from upstream to downstream with mean average value of 5.02 mg/L, 3.02 mg/L, 2.10 mg/L, and 1.27 mg/L, respectively, according to their abundance (Table 3). Similarly, anions for KRB such as HCO_3^- , Cl^- , SO_4^{2-} and NO_3^- varies from 6.52 to 30.95 mg/L, 1.93–17.12 mg/L, 0.73–5.35 mg/L, and 0.62–2.5 mg/L, respectively, with average value of 14.91, 6.18, 2.18 and 1.72 mg/L (Table 3) respectively. Coming to VRB the Na, Ca, K, and Mg in river water vary in the range 1.09–6.98 mg/L, 1.05–3.27 mg/L, 0.69–2.63 mg/L, and 0.56–2.91 mg/L, respectively, from upstream to downstream with a mean average value of 4.03 mg/L, 2.16 mg/L, 1.66 mg/L, and 1.74 mg/L, respectively, according to their abundance (Table 3). Similarly, anions such as HCO_3^- , Cl^- , SO_4^{2-} , and NO_3^- varies from 4.03 to 20.58 mg/L, 0.89–6.29 mg/L, 0.81–2.55 mg/L, and 0.13–1.03 mg/L, respectively, with average value of 12.31, 3.59, 1.68 and 0.58 mg/L (Table 3). The mean value of abundant cations (Na and Ca) and anions (HCO_3^- and Cl^-) are compared with the world, Indian and western ghat rivers. It is found that Na value of KRB is almost like the MRB (5.61 mg/L)⁸⁶ and smaller than peninsular rivers like Narmada, Godavari, Bhima and Tapi (Table 3). However, they are higher than world largest rivers viz. Amazon, Loire, and Orinoco (Table 3). Further, the Ca value of KRB is comparable with the Orinoco (3.26 mg/L) though the latter is slightly higher than the former (Table 3). Moreover, the Ca value reported in KRB is much less than several peninsular rivers (Table 3), and some WGs rivers viz. Periyar, Pambar and Muthirapuzha (Table 3) and slightly less than world's largest river Amazon (5.58 mg/L)⁸⁷. The HCO_3^- mean concentration is much less than Peninsular rivers (Table 3), Kali river (53.44 mg/L)⁶⁴, Pambar (71.44 mg/L)⁶¹ and Muthirapuzha river (51.31 mg/L)⁸⁶. However, average HCO_3^- in KRB is higher in concentration compared to Manimala⁵⁶, Achankovil⁵⁹, and Orinoco rivers⁸⁸. While the average Cl value (6.18 mg/L) of KRB is compared to the Krishna river (6.82 mg/L)⁷⁹ and is higher than World's largest rivers (Table 3). However, they are considerably less than some WGs rivers Manimala, Periyar, Pambar, Muthirapuzha, and Achankovil, western ghat river like Netravati and Peninsular rivers like Bhima, Godavari, and Tapi (Table 3). When comparing VRB, with other rivers all around the world including KRB and other western ghat rivers, the mean value of hydrochemical variation is less compared to other river basins owing to the pristine nature and more or less a most of the basin flows through a midland region where developments are still on the path while the KRB flows through the developed urban portion of the Trivandrum city.

Similar to dissolved load chemistry, TSS estimation of the river is carried out seasonally. The TSS in the KRB ranges from 0.69 to 15.42 mg/L, 2.74–34.12 mg/L, and 1.8–23.18 mg/L for the PRE, MON, and POM seasons respectively with an average discharge weighted average value of 25.03 mg/L at the outlet. Similarly, the TSS in the VRB ranges from 0.2 to 11.6, 2.39–16.28, and 3.1–8.1 for PRE, MON, and POM respectively with a discharge weighted average of 12.02 mg/L at the outlet. Though the TSS increases downstream, at some particular locations it shows higher values than the rest of the region for both rivers. The TSS levels in the KVRB are notably lower than those of several river basins in the Western Ghats and other regions. For instance, the TSS concentration in the KVRB is lower than those recorded in the Western Ghat rivers Pambar River (14.64 mg/L)⁶¹ and the Kuzhankal River (44.82 mg/L)⁸⁹. When compared to larger river systems, the TSS in the Mahanadi River (45.25 mg/L)⁹⁰, Padma River (120.82 mg/L)⁹¹, and several Himalayan rivers such as the Ghagra (255.5 mg/L)⁹², Gandak (568 mg/L)⁹², and Son (120 mg/L)⁹² is significantly higher. Additionally, other river basins such as the Damodar River (47.29 mg/L)⁹³ and Siang River (109.55 mg/L)⁹⁴ also show higher TSS values compared to the KVRB. This indicates a relatively low suspended sediment load in the KVRB compared to these other river systems.

Geochemical processes controlling the dissolved load

The Gibbs diagram (Fig. 2) of KVRB illustrates that the samples from all three seasons of both rivers fall between the precipitation dominance and rock dominance categories. In particular, most of the upstream samples in all seasons are dominated by precipitation, whereas the middle to downstream samples, except for VRB-MON, are governed by water-rock interaction, i.e., chemical weathering. The preponderance of precipitation in VRB-MON samples was due to decreased total dissolved solids (TDS) resulting from continuous monsoon rainfall, making precipitation the predominant factor in these samples. Further, the relative contribution of these processes is elucidated via the correlation between diverse dissolved elemental species, illustrated through different bivariate plots. In the seasonal bivariate plot (Fig. 3a) for KVRB, the linear relationship between $\text{Na} + \text{K} + \text{Ca} + \text{Mg}$ and HCO_3^- suggests silicate weathering, while deviations from the 1:1 line indicate additional cation inputs from sources such as atmospheric and anthropogenic influences. This addition is mostly observed in PRE season as the concentration of ionic species is enriched in this season. The proton source for the chemical weathering is unraveled by plotting the HCO_3^- vs. $\text{CO}_3 + \text{SO}_4$ (Fig. 3b) diagram as this diagram specifies whether carbonic acid and sulphuric acid are responsible for weathering. The HCO_3^- vs. $\text{HCO}_3^- + \text{SO}_4$ diagram plot for both rivers shows that some of the samples from all seasons fall along the 1:1 line and some move toward the $\text{HCO}_3^- + \text{SO}_4$ axes, indicating the presence of both carbonic acid as well as sulphuric acid presence in chemical weathering. However, the proton source in the study area is carbonic acid since there are no extensive SO_4 contributing rock/mineral sources, such as pyrites, despite their minimal presence in some regions of the upstream part of the study area. Furthermore, the deviation towards the $\text{HCO}_3^- + \text{SO}_4$ is attributed to relatively minor contributions of SO_4 from atmospheric and anthropogenic sources that appear to be increasing downstream. The aforementioned diagrams describe the weathering and proton source for the KVRB, emphasizing the significance of categorizing rock weathering (silicate or carbonate) as explained by the $\text{Na} + \text{K}$ vs. $\text{Ca} + \text{Mg}$ (Fig. 3c) bivariate plot. The $\text{Na} + \text{K}$ vs. $\text{Ca} + \text{Mg}$ diagram shows that all the samples fall away from the 1:1 line except for a few samples in monsoon signify the silicate weathering and absence of carbonate weathering in the watershed. This also signifies that other sources are controlling the Na and K concentration in KVRB like atmospheric and anthropogenic. Moreover, the findings from previous geochemical studies in the area, coupled with field visits conducted during the current study, support and validate this conclusion (Fig. 1).

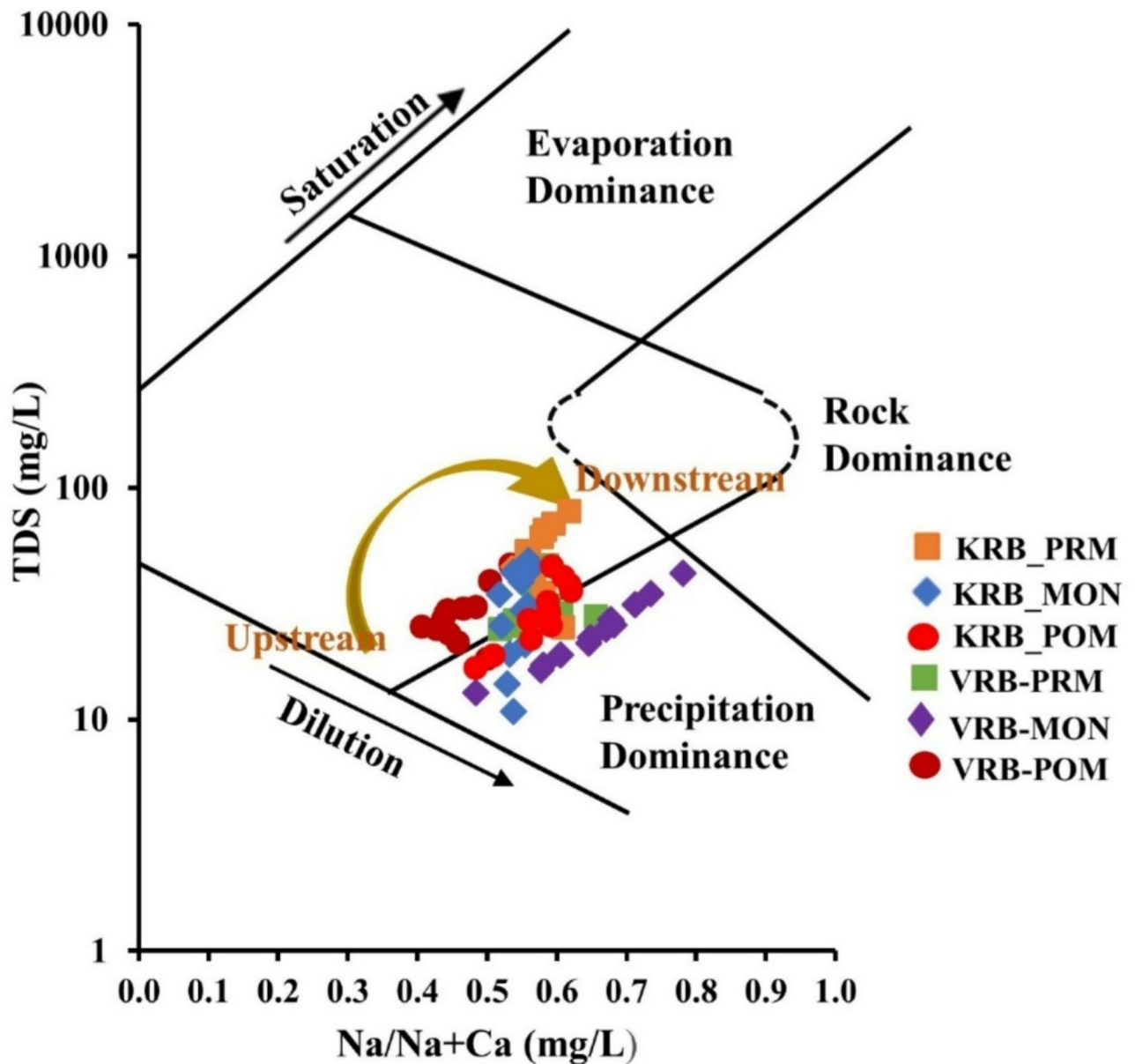


Fig. 2. Gibb's diagram of KVRB; Identifies the dominant soult acquisition mechanisms.

Further, the Na vs. Cl plot (Fig. 3d) for KVRB shows dominance of Na over Cl, and also Na/Cl value of all samples is over 1 indicating the presence of another source for Na like silicate weathering and anthropogenic effect in the region. Additionally, the increment of Cl towards the downstream station indicates the possibility of anthropogenic activities in the watersheds, which is evident from Fig. 3e which shows Cl addition in every season towards downstream as there is no Cl rock source (halite) present in the study area (Fig. 1). The rise of anthropogenic activities towards downstream is distinguished from the Na/Cl vs. Cl diagram plot for both KVRB (Fig. 3f). The diagram shows that most of the samples especially pre-monsoon and monsoon samples falls above the standard line plot for marine contribution line ($\text{Na/Cl} = 0.86$) as well as parallel to the Cl axes signify the role of anthropogenic activity in the KRB. Nevertheless, the samples above the marine standard line and parallel to Na/Cl signify the role of silicate weathering in the region. Additionally, some samples show equal contributions of both sources. The contribution of chemical weathering from rock sources is more comprehensively explained in the subsequent section.

Na normalized mixing diagram

The two end-members, rock and soil with weathered profile, of KVRB lie well above the silicate end-member of Gaillardet et al.²⁴. The average rock end member of the KVRB (i.e., $\text{Ca/Na} = 0.9 \pm 0.21$ and $\text{Mg/Na} = 0.43 \pm 0.17$) is approximately twice as high as the average end member reported by Gaillardet et al.²⁴ (i.e., $\text{Ca/Na} = 0.35 \pm 0.15$, $\text{Mg/Na} = 0.24 \pm 0.12$), owing to local lithological variations. Specifically, the KVRB is drained through granulate-

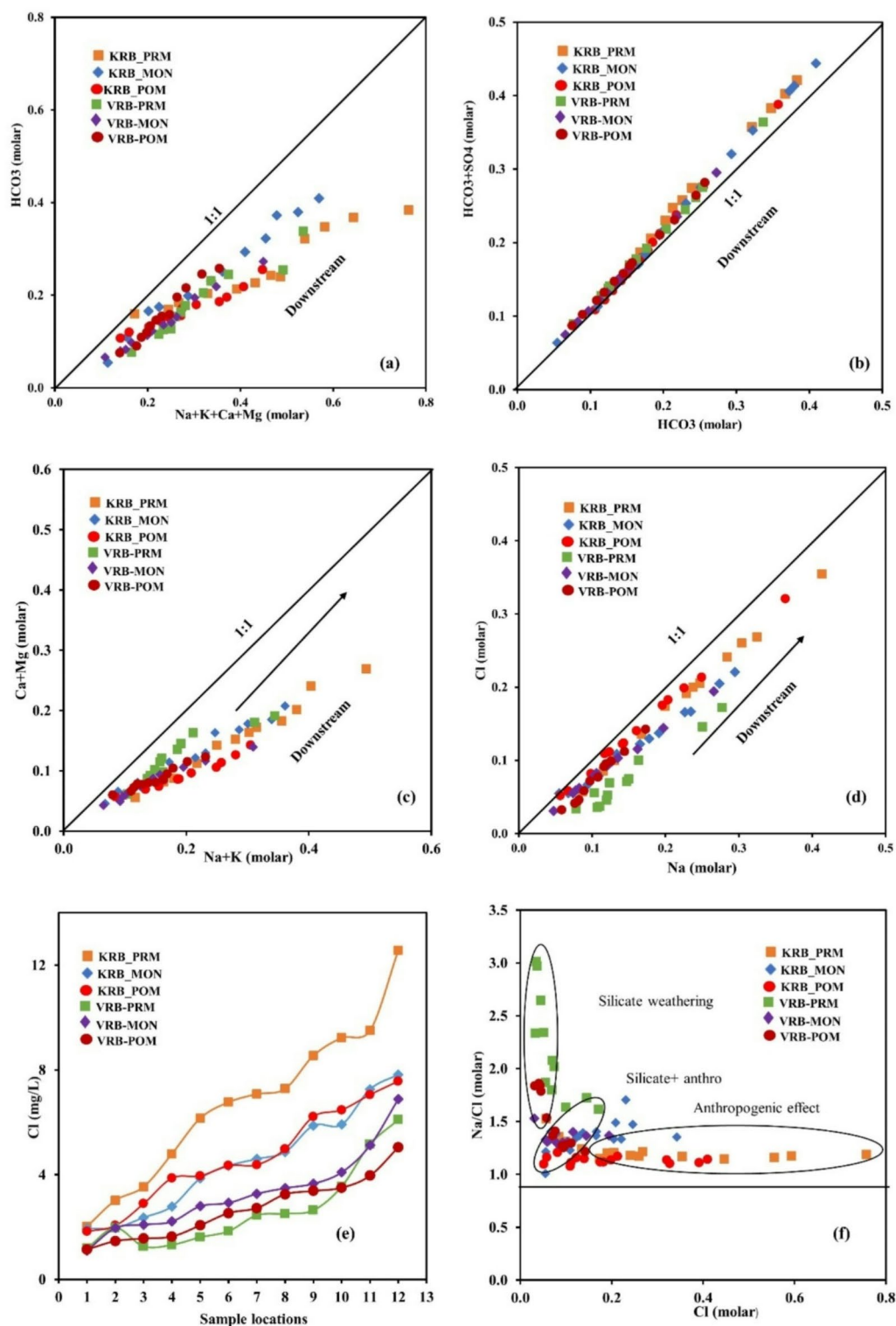


Fig. 3. Bivariate diagrams of KVRB. (a) Na + K + Ca + Mg vs. HCO₃ diagram representing the chemical weathering of the region (b) HCO₃ + SO₄ vs. HCO₃ confirms the proton source of the region (c) Na + K vs. Ca + Mg confirms the dominance of silicate weathering (d) Na vs. Cl confirms other source of Na like anthropogenic activities (e) location vs. Cl shows increasing effect anthropogenic towards downstream (f) Na/Cl vs. Cl signify role of silicate weathering.

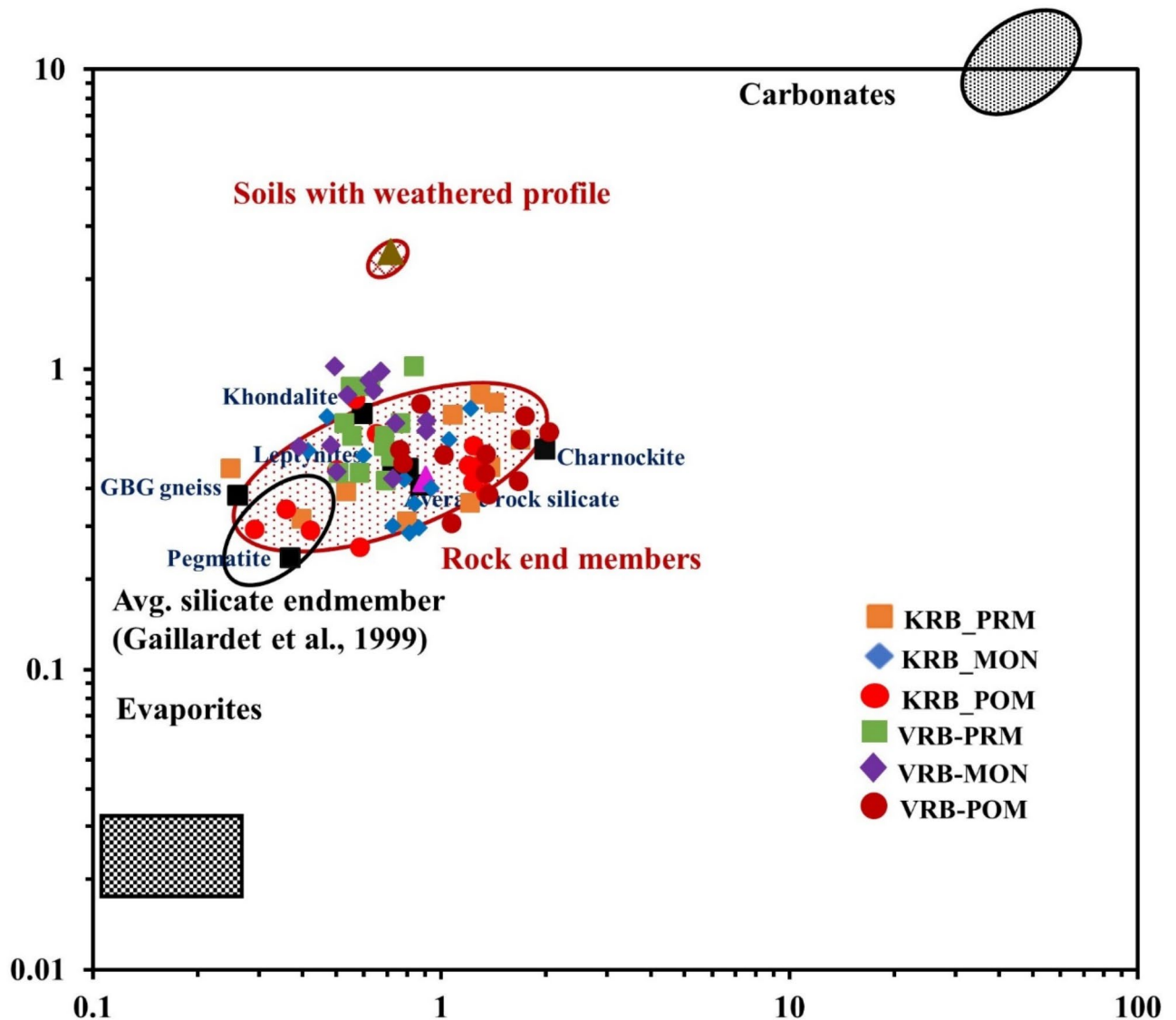


Fig. 4. End-member mixing diagram of KVRB modified after Gaillardet et al. (1999) to incorporate the dominant lithological characteristics of the KVRB.

dominated lithology, resulting in higher Na-normalized ratios compared to the average crystalline rocks^{24,26}. Thus, this study demonstrates the local geo-environmental factors, that can affect the hydrochemistry viz. lithology, soil, and weathered profile. Here, the Na-normalized Ca versus Mg of KVRB (Fig. 4) is plotted along with water samples only after removing the other source contributions like atmospheric and anthropogenic for all the water samples. The Na-normalized Ca versus Mg of KRB shows an overall dominance near the silicate end-member of rocks for most of the water samples of three seasons with a wide spread among the dominant lithologies indicating the silicate weathering of rocks controlling the hydrochemistry of the basin. According to the mixing diagram, silicate end-members such as leptynites, biotite gneiss, khondalites, and charnockites contribute most of the ions to the water especially the leptynites and khondalite, which are also the dominant rock group (Fig. 1) found in the basin and are easily susceptible to weathering⁹⁵. However, some of the samples in all three seasons show an inclination towards the lithology indicating the underlying rock weathering dominance for that sample rather than the mixing contribution from various lithologies. Thus, from the end-member mixing diagram, it can be concluded that the silicate end-member dominates the hydro-geochemistry of the KRB for all three seasons with almost no effects from the soil with weathered profile end-member as well as the evaporates and carbonates.

Quantification of KVRB: source-wise input to the dissolved load

The quantification of dissolved sources of KVRB is done based on the aforementioned methodology described in the materials and methodology Sect.

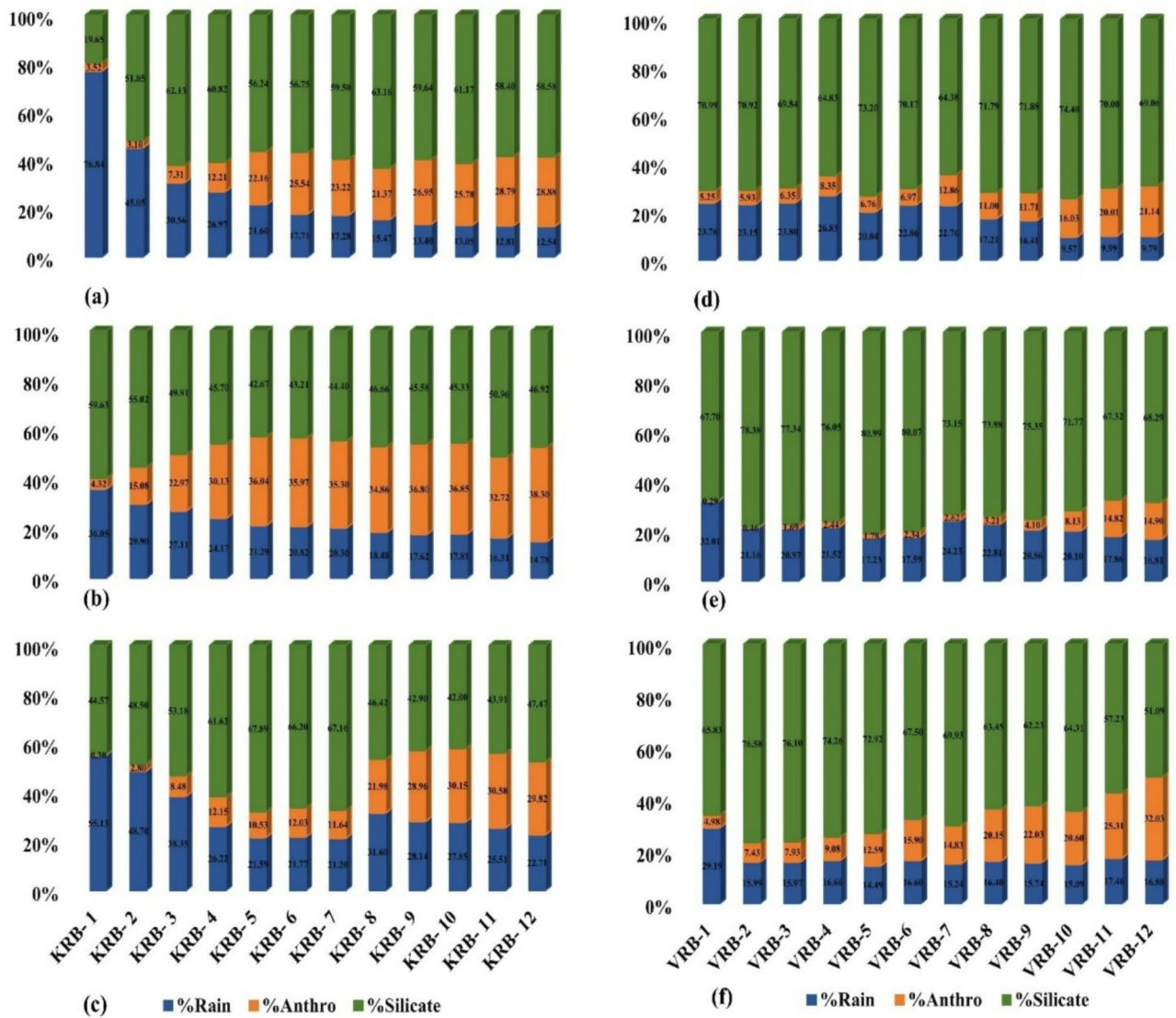


Fig. 5. Source-wise solute load contributions to the total dissolved load of KRB and VRB from atmospheric input, silicate weathering, and anthropogenic sources (a) KRB-PRM (b) KRB-MON (c) KRB-POM (d) VRB-PRM (e) VRB-MON (f) VRB-POM.

Atmospheric

The atmospheric contribution to the KRB varies significantly across seasons, ranging from 14.78 to 76.84% (Fig. 5). During the pre-monsoon (PRM) season, it ranges from 36.05 to 76.84% (Fig. 5a); in the MON season, it ranges from 12.54 to 76.84% (Fig. 5b); and in the POM season, it ranges from 12.69 to 55.10% (Fig. 5c). The lowest contribution, 14.78%, is observed during the PRE season at the downstream location (Maruthoorkadavu, KRB-12), while the highest contribution, 76.84%, occurs during the monsoon season in the upstream region near the Peppara Dam (KRB-1). The discharge-weighted mean average contribution for the entire basin at the outlet (Maruthoorkadavu, KRB-12) is 14.96% (Fig. 6a).

Similarly, the atmospheric contribution to the VRB ranges from 9.57 to 32.01% for all seasons. Among the three seasons the atomic contribution of PRM season range from 9.57 to 23.76% (Fig. 5d), and for MON season it is in the range between 16.81 and 32.01% (Fig. 5e) while for POM it ranges between 15.09 and 29.19% (Fig. 5f). The lowest contribution, 9.57%, is observed in the pre-monsoon season at the downstream location (Karett, VRB-10), while the highest contribution, 32.01%, occurs during the monsoon season in the upstream region (Kallar eco-tourism area, VRB-1). The discharge-weighted mean average contribution for the entire basin at the outlet (Poovanpara, VRB-12) is 15.86% (Fig. 6a), with the peak value recorded in the Kallar eco-tourism region, renowned for its pristine environment.

When comparing the weighted yearly average contributions at the outlets of KRB and VRB, it is found that though the upstream of KRB is mostly affected by a sample relies on atmospheric contribution compared to the VRB, both of their outlet contribution are almost similar, viz. this decreases significantly to 13.89% at the

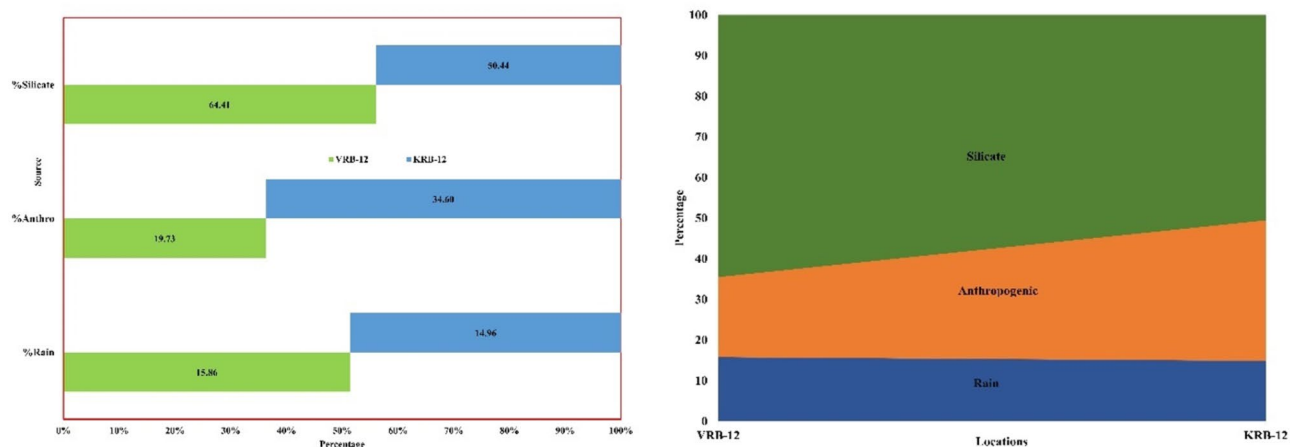


Fig. 6. (a) Discharge weighted yearly average (b) Comparison diagram of KRB and VRB.

outlet. This is almost like the 15.86% contribution of VRB at its outlet. This suggests that additional sources are contributing more to the dissolved load in KRB beyond atmospheric contributions, unlike in VRB (Fig. 6b).

Anthropogenic input

The estimated anthropogenic input for KRB reveals a yearly discharge-weighted average value of 34.60% at the basin's outlet. However, the contribution of anthropogenic input to dissolved load at each location from upstream to downstream and the seasonal contribution may show significant variation due to the dilution effect in water from different sources. In the PRE (Fig. 5a), contribution from the anthropogenic source ranges from 4.32% in the Upstream (Peppara) to 38.30% of the downstream (Marathoorkadavu) location; whereas in the POM (Fig. 5c) it ranges from 0.36% (Peppara) to 62.66% (Marathoorkadavu); signify the role of anthropogenic activities in the downstream region. However, the MON samples of (Fig. 5b) upstream show slightly higher anthropogenic contribution (3.10%) compared to the POM. However, the downstream portion shows comparatively a lesser amount (28.88%) of anthropogenic contribution in MON due to the mixing of fresh water with other sources and due to the high discharge of water throughout the basin. The slightly higher contribution of anthropogenic TDS in the MON samples from the upstream region, compared to POM, is likely due to increased runoff during sample collection, which led to a rise in TDS concentration. This runoff could have introduced additional dissolved solids from anthropogenic sources, contributing to the observed increase.

The anthropogenic contribution of VRB is significantly less compared to the KRB. The variation of anthropogenic contribution from upstream to downstream for different seasons are showed in the Fig. 5. The PRE and POM samples contribution vary in the range 5.25–21.14% (Fig. 5d) and 4.98–32.03% (Fig. 5e) respectively, towards the downstream while the MON samples (Fig. 5f) variation of contribution is less (0.29–14.90%). Further, the discharge-weighted yearly average shows a contribution of 19.73% (Fig. 6a) at the outlet. Comparing the yearly weighted average of both KRB and VRB, it is found that the contribution of anthropogenic activity to the dissolved load is less observed in VRB (Fig. 6b). Though both river basin flows through the southern part of Kerala and is showing almost nearly climatic conditions, developmental activities are actively and rapidly happening in the KRB as it flows through the corporation area of Trivandrum district^{78,96}.

Silicate weathering

The approximated silicate weathering contribution of KRB varies considerably from upstream to downstream propounding the silicate weathering dominance over the area. Based on silicate contribution estimation to the entire dissolved load from upstream to downstream, the values range from 42.67 to 59.63%, 19.65–63.16%, and 42–67.89% for different seasons namely PRE (Fig. 5a), MON (Fig. 5b), and POM (Fig. 5c), respectively, with a yearly average whole basin discharge weighted value of 50.44% at the outlet, which suggest that the silicate weathering input is dominant over the KRB. Similarly, the silicate weathering contribution of VRB at the outlet is estimated as 64.38–74.40%, 67.70–80.99%, and 51.09–76.58% for the PRE, MON, and POM, respectively with an average discharge weighted value of 64.41% (Fig. 6a). This fact agrees with the mixing analysis explained in the previous section.

Likewise, the contribution of silicate weathering for VRB is estimated seasonally. The seasonal analysis shows the gradual increment in silicate contribution towards downstream except in some regions. This is attributed to the anthropogenic dominance over the respective regions. For example, the mouth downstream samples VRB 11 and VRB 12 show slightly less contribution compared to the preceding midland contribution due to the increased anthropogenic contribution in both the sites irrespective of the season. The PRE contribution varies in the range of 64.38–74.40% (Fig. 5d); the MON is in the range of 67.32–80.99% (Fig. 5e) while the POM is in the range of 51.09–76.58% (Fig. 5f) with a yearly weighted average of 64.41% (Fig. 6a) at the outlet. This value suggests that the dissolved load chemistry of VRB is ruled by silicate weathering contribution and is at the forefront compared to VRB.

The quantification analysis of KVRB shows that the dissolved load chemistry is controlled by silicate weathering followed by anthropogenic and atmospheric contribution respectively. However, the silicate weathering contribution is more observed in the VRB compared to the KRB (Fig. 6b). This is due to the anthropogenic activities and topographical aspects prevailing in the KRB region.

Chemical weathering rates and CO₂ consumption rates

Silicate weathering rates (SWR)

The estimated silicate weathering value of the KVRB varies across different seasons, exhibiting a discharge-weighted average of 30.96 t km⁻² yr⁻¹ and 22.89 t km⁻² yr⁻¹ for KRB and VRB respectively. This suggests that weathering rates in the KRB region is comparable to other Western Ghats rivers such as Gurupur (38 t km⁻² yr⁻¹)²⁶ and Chandragiri–Payaswini (39 t km⁻² yr⁻¹)⁶², while VRB is comparable to the Muvatupuzha (27 t km⁻² yr⁻¹)⁹⁷, Sharavati (27 t km⁻² yr⁻¹)⁶³, and both are lower than Gad (40 t km⁻² yr⁻¹)⁷⁹. However, the KRB is comparable to the Godavari (34.69 t km⁻² yr⁻¹)¹⁴ and Tapti (33.6, t km⁻² yr⁻¹)⁹⁸, while VRB is exhibiting low value. Similarly, the SWR of KRB exhibits similar attributes with the peninsular rivers like Narmada (33.9 t km⁻² yr⁻¹)³ and Swarnamukhi (30.57 t km⁻² yr⁻¹)⁴, while VRB possesses low. Moreover, KVRB has much higher rates compared to some largest river basins in the world shown in Table 4. Being small tropical mountainous rivers, the SWR of KVRB is comparable to other larger of basins of Western Ghats, Peninsular as well as the World's

Basin	Discharge Km ³ /year	Area (10 ³ m ²)	SWR (t km ⁻² yr ⁻¹)	CO ₂ _{sil} (10 ¹⁵ molkm ⁻² year ⁻¹)	Reference
Amazon	6590	6112	13	0.52	Gaillardet et al. ²⁴ (1999)
Amazon			23		Mortatti & Probst ⁸⁷ (2003)
Mississippi	580	2980	3.8	0.7	Gaillardet et al. ²⁴ (1999)
Yangtze	928	1808	5.5	0.6	Gaillardet et al. ²⁴ (1999)
Changjiang			2.45	0.8	Chetelat et al. ⁴² (2008)
Mackenzie	308	1787	1.8	0.34	Gaillardet et al. ²⁴ (1999)
Red	123	120	27.5	6.83	Moon et al. ⁹ (2007)
Upper Han	41.1	95	5.6	1.01	Li et al. ¹⁰⁴ (2009)
Huanghe	28.3	752	3.23	0.35	Fan et al. ¹⁰⁵ (2014)
Mekong	470	795	10.2	1.91	Li et al. ³⁶ (2014)
Kajili			48	5.8	Das et al. ⁷⁹ (2005)
Xijiang			16.6	3.6–6.7	Sun et al. ¹⁰⁶ (2010)
Congo			4.3	0.5	Gaillardet et al. ²⁴ (1999)
Nile			0.8		Gaillardet et al. ²⁴ (1999)
Parana				0.9	Gaillardet et al. ⁵ (1995)
Sorocaba, Brazil				2	Fernandes et al. ¹⁰⁰ (2016)
Himalayan					
Brahmaputra	510	580	10.3	1.5	Gaillardet et al. ²⁴ (1999)
Ganges	493	1050	14	4.5	Gaillardet et al. ²⁴ (1999)
Ganga, Rishikesh	22.4	20	12.9	3.8	Krishnaswami & Singh ³³ (1998)
Indus	90	916	3.8	0.6	Gaillardet et al. ²⁴ (1999)
Kali river			41.3	2.9	Arun et al. ⁶⁴ (2022)
Yamuna	10.8	10	28	7	Dalai et al. ⁵² (2002)
Peninsular					
Narmada		89	33.9	21.2	Sharma et al. ⁹⁸ (2008)
Swarnamukhi	5.39	3	30.57	8.77	Patel et al. ⁴ (2020)
Kaveri, Musiri	8.5	66	7.9	2.6–3	Pattanaik et al. ⁹ (2013)
Gad			40	5.7	Das et al. ⁷⁹ (2005)
Tapti		61	33.6	18.1	Sharma & Subramanian (2008)
Krishna		36	14	4.2	Das et al. ⁷⁹ (2005)
Bhima		34	12	3.3	Dalai et al. ⁵² (2002)
Sharavati			27	3.9	Amrith et al. ⁶³ (2022)
Godavari	110	310	34.69	5.8	Jha et al. ¹⁴ (2009)
Nethravati	12	4	42	2.8–2.9	Gurumurthy et al. ²⁶ (2012)
Gurupur			38	5.2	Gurumurthy et al. ²⁶ (2012)
West flowing western ghat coastal					
Chandragiri–Payaswini			39	8.95	Nisha et al. ⁶² (2021)
Muvatupuzha			27	5.5	Trivikramaji & Joseph ⁹⁷ (2001)

Table 4. The SWR and CCR of the World's, Himalayan, Peninsular, and Western Ghats West flowing coastal rivers.

largest rivers signifying the role of these tropical mountainous rivers in controlling dissolved flux to the sea. This study gives the conuntenence to the findings put forward by Milliman⁵⁵. The higher silicate weathering rates of KVRB are due to the orogenic factors (steep slopes), rainfall, and humid nature compared to other regions. The small difference in the estimated SWR value of KRB and VRB can be attributed to the region's topographical difference and rainfall dynamics as VRB mostly flows through midland rather than KRB and has a gentle slope compared to the KRB.

CO₂ consumption rates (CCR)

The CCR estimated for KRB and VRB at the outlet named Maruthoorkadavu and Poovanpara is expressed as 1.16×10^6 mole $\text{km}^{-2} \text{yr}^{-1}$ and 3.20×10^5 mole $\text{km}^{-2} \text{yr}^{-1}$ by using appropriate conversion factors. Further, this value of KRB is much higher than some of the World's river rivers, including Amazon (0.52×10^5 mole $\text{km}^{-2} \text{yr}^{-1}$)²⁴, Red (6.83×10^5 mole $\text{km}^{-2} \text{yr}^{-1}$)⁹⁹, Changjiang (0.8×10^5 mole $\text{km}^{-2} \text{yr}^{-1}$)⁴², Sorocaba (2×10^5 mole $\text{km}^{-2} \text{yr}^{-1}$)¹⁰⁰. It is also higher than the rates observed in Himalayan rivers^{24,33,52,64}, Krishna (4.2×10^5 mole $\text{km}^{-2} \text{yr}^{-1}$)⁷⁹, Swarnamukhi (8.77×10^5 mole $\text{km}^{-2} \text{yr}^{-1}$)⁴, Godavari (5.8×10^5 mole $\text{km}^{-2} \text{yr}^{-1}$)¹⁴, and even higher than the west-flowing Western Ghats rivers that drain through Basaltic terrain and Dharwar craton (Table 4) including the current estimation of VRB. This must be attributed to the topographical characteristics of the region such as slope and granulitic terrain, easily susceptible to erosion and weathering⁹⁵ compared with the climatic conditions prevailing in the KRB. Moreover, the other studies have utilized the World's average rock ratios for the creation of end-members and for estimating the SWR and CCR values, but the current study uses the rock ratios of the prevailing rock composition present in the area where we have collected and analysed the predominant lithological samples of KRB. This resulted in higher Na-normalized Ca and Mg ratios for the silicate end-members and thus, higher silicate weathering flux there by the higher SWR and CCR values. The higher disparity between CCR values of KRB and VRB is attributed to the topographical difference and human influence in the KRB basin.

Uncertainties in Estimation of SWR and CCR

The evaluation of silicate weathering and its climatic influences in a catchment is subject to various uncertainties. These uncertainties primarily arise from estimating riverine chemical inputs, influenced by sampling strategies, site selection, laboratory methods, instrument calibration, and the reliability of correction procedures and estimation models^{85,99}. Mitigating these uncertainties is essential for obtaining the accurate results. Sampling sites were chosen to account for spatial variability in geology, land use, and topography, as well as to mitigate saline water intrusion near the coast. Samples were collected sufficiently upstream of river outlets to minimize coastal influences and were positioned downstream of tributary confluences to capture their contributions to the river chemistry. These decisions ensured that the data represent the catchment's chemical profile comprehensively. To avoid contamination from saline water intrusion, sampling was conducted upstream of coastal areas. This ensured that the observed riverine chemistry predominantly reflected terrestrial processes and not external marine influences.

To ensure accuracy, instruments were regularly calibrated, and quality control measures were implemented during laboratory analysis. Hydrochemical data were corrected using the Normalized Inorganic Charge Balance (NICB) method, as detailed in materials and methodology Sect. This correction addressed ionic discrepancies and improved the reliability of chemical measurements used in source attribution.

Assigning chemical contributions to various sources, including atmospheric inputs, anthropogenic influences, and silicate weathering, is a significant source of uncertainty. These contributions were addressed as follows; (1) **Atmospheric Contributions:** Due to insufficient direct data, the minimum chloride concentration from upstream regions was used as a proxy for atmospheric inputs, assuming negligible influence from other sources in the area. (2) **Anthropogenic Influences:** These were estimated based on theoretical models and local land use data, ensuring consistency with the catchment's background chemical composition. (3) **Silicate Weathering:** To minimize uncertainty, site-specific geochemical data including local lithological, weathered profile, and soil samples (described in methodology and results sections) and were used instead of generalized models, such as the Gaillardet et al. (1999) mixing diagram, which may not adequately reflect local conditions, especially in the present case where there are no carbonates and halite mineral deposits. This study emphasizes the importance of addressing uncertainties in assessing SWR, CCR and its drivers. Even then, the minimized uncertainties would have carried out forward from the geochemical and hydrochemical analytical results of the soil, water, sediment, and rock samples. The estimated uncertainties in the SWR and CCR varies in the range of 3 to 7% of their absolute values depending upon the season and location of KVRB. By implementing a systematic approach to sampling, applying rigorous data correction methods, and relying on locally derived geochemical data, we have minimized errors and enhanced the reliability of the findings. These practices provide a robust framework for improving the precision of weathering flux assessments in diverse catchments.

Temperature effects on silicate-weathering rates

The rising of temperatures over the Earth's surface impels us to investigate its effect on silicate weathering, a process that plays a crucial role in climate regulation^{85,101}. Gurumurthy et al.²⁶ mentioned that rivers draining through silicate basement, combined with elevated temperature (30 °C) and high runoff levels (3300 mm. y^{-1}), can drive intense silicate weathering. Similarly, Reddy et al.⁵⁷ state that the west-flowing Western Ghats rivers characterized by high runoff, elevated temperatures, humid climates, and distinct topographical features promote enhanced chemical weathering characteristics of the basin. As mentioned in the study area Sect. the tropical mountainous KVRB also falls under this category and exhibits high SWR values. Hence, it is essential to assess the weatherability of silicate rock with temperature, where the weathering rate and temperature are related by the Arrhenius equation (silicate weathering rate (SWR) versus $1/T$) as mentioned in Eq. (13).

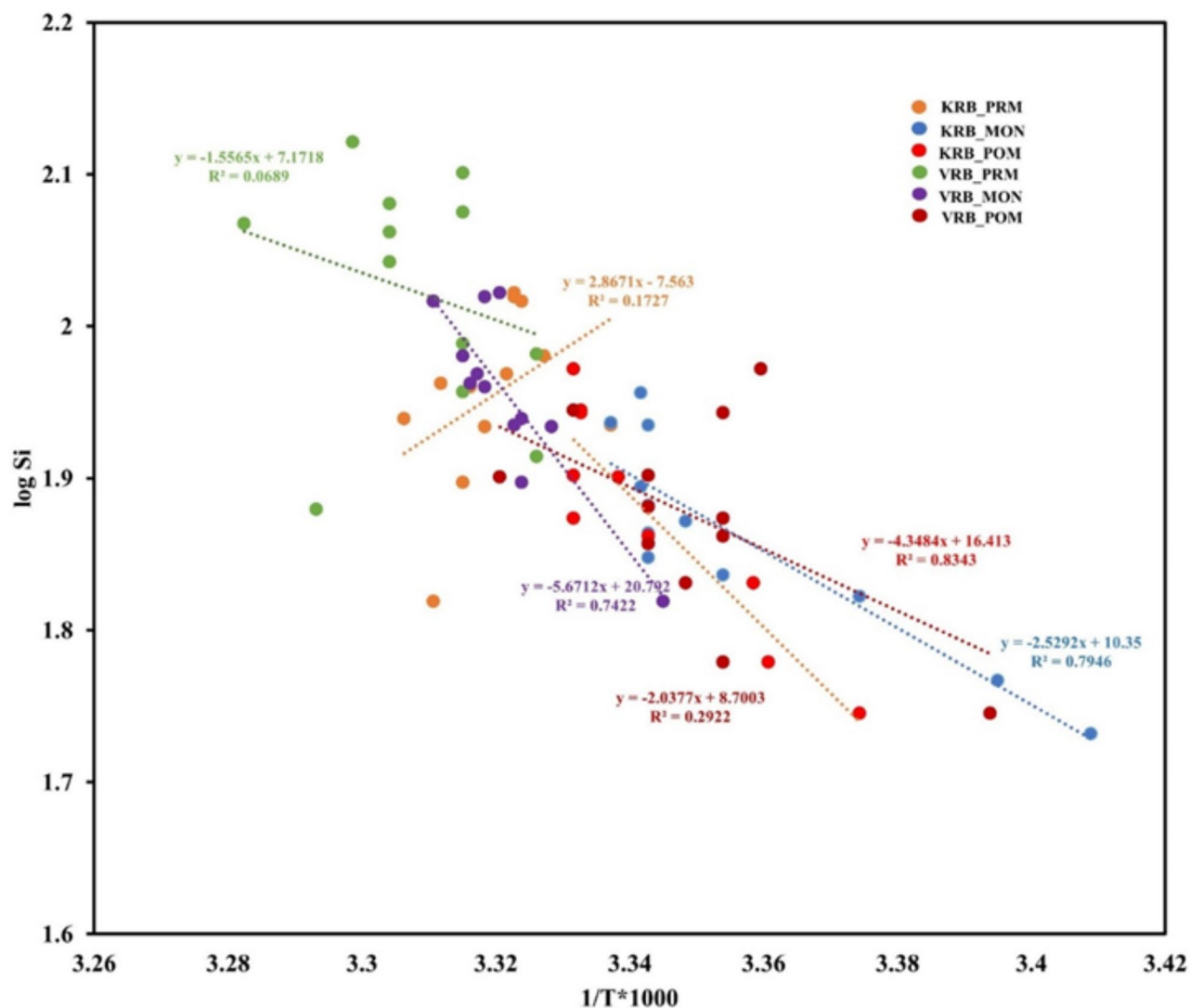


Fig. 7. Arrhenius plots of inverse of water temperature (1/T) vs. log Si. The significant correlation is suggestive of the moderate dependence of silicate weathering on temperature.

$$\text{SWR} = A \cdot \exp(-E_a/RT) \quad (13)$$

Where, 'SWR' is the silicate weathering rate, 'A' - Arrhenius constant, ' E_a ' - activation energy, 'T' - temperature, and 'R' is the universal gas constant. Thus, the activation energy of the dissolution (weathering reaction) of a particular mineral is determined by the set of following equations assuming that the silicate minerals release silica (SiO_2) via the dissolution process following the first-order kinetics using the Arrhenius Eq.

$$\text{Log}(\text{Si}) = \text{Log}A - E_a/RT \quad (14)$$

Here, Si is the molar concentration of silica and A, E_a , R, T are the Arrhenius parameters. By using measured silica concentrations at different places and the corresponding temperatures in the KVRB (Table 1), the Log (SiO_2) versus 1/T is plotted (Fig. 7) with appropriate conversion values where the slope of the plot and the E_a are given by the following Eq.

$$\text{Slope} = -E_a/R, \text{ and thus, } E_a = \text{slope} \times R \quad (15)$$

The current study analyzes the temperature dependence on Si by plotting the Arrhenius plot to understand silicate weathering as it is the most abundant and resistant mineral on the earth. The Arrhenius plot for the KVRB demonstrates that seasonal fluctuations significantly affect ion release into the water, underscoring the critical role of temperature in the weathering process. This seasonal analysis helps to elucidate the influence of temperature variations on weathering rates.

In the KRB, the correlation between temperature and silica release varies across seasons, with coefficients of 0.17 for the PRE, 0.79 for the MON, and 0.83 for the POM, as illustrated in Fig. 7. Similarly, in the VRB, the correlation coefficients are 0.06 for the PRE, 0.74 for the MON, and 0.29 for the POM samples. Despite these seasonal differences, the overall correlation coefficients of 0.59 for KRB and 0.56 for VRB point to a moderate influence of temperature on silica release, suggesting ongoing weathering in both river systems.

The estimated activation energies for silicate weathering are 27 kJ/mol in KRB and 25 kJ/mol in VRB, which are notably lower than those found in other river systems, such as the Himalayan Yamuna River (51 kJ/mol) and rivers dominated by basalt weathering, like those studied by Dessert et al.¹⁰². These lower activation energy values indicate a higher dissolution rate of the silicate minerals in the granulite bedrock of the KVRB region, contributing to more efficient weathering.

The moderate effect of temperature on silica release, along with a high rate of silicate weathering, can be explained by several interrelated factors. Although temperature can speed up chemical reactions, its influence on silica release is generally less pronounced than other weathering factors, such as mineral type, water availability, and prevailing environmental conditions. In regions characterized by high silicate weathering rates, the primary processes are often driven by abundant rainfall and intense water-rock interactions, which promote the breakdown of silicate minerals. As a result, even with moderate fluctuations in temperature, the significant weathering rates can still lead to considerable silica release due to the stronger influence of these environmental factors¹⁰³.

In this context, the moderate dependence of silica on weathering can be linked to seasonal differences. The PRE samples from the KVRB and the POM samples from VRB showed significantly lower correlation values than the MON samples from KVRB and POM from KRB. This notable variation in correlation coefficients between the two seasons explains the overall moderate influence of temperature on silica release. Additionally, it highlights the importance of climatic fluctuations in silicate weathering; these fluctuations are more prominent during the monsoon season, while they tend to be less apparent in the pre-monsoon season.

The increased weathering tendency in the study area is primarily due to its geological setting, where the reactive granulite silicate bedrock is more susceptible to dissolution. Moreover, factors such as the region's steep terrain, heavy rainfall, and high humidity intensify weathering by promoting water-rock interactions and accelerating chemical breakdown processes.

The findings from this study highlight the intense nature of silicate weathering in the KVRB, driven by both the low activation energy of the granulite bedrock and the region's favorable climatic and topographic conditions. The moderate but consistent influence of temperature across seasons reinforces the role of temperature as a key factor in controlling weathering rates. Overall, the KVRB exhibits a greater propensity for silicate weathering compared to other river systems, contributing to the ongoing geochemical evolution of the landscape.

Physical Weathering Rates (PWR)

The topographical and climatic characteristics, along with the estimated AE for the KVRB samples and the observed variation in TSS in both the KRB and VRB, highlight the importance of assessing the physical weathering rate (PWR) of the basin. In this study, TSS is utilized as a key indicator to evaluate the rate of physical erosion. The concept of PWR estimation using TSS has been adapted following the³⁵. The estimation of KVRB done using the same as the SWR estimation reported in methodology Sect. of the current study and the equation can be written as

$$PWR = (Q/A) \times [TSS]$$

Similar to SWR, here, the Q, and A respectively represent the discharge and Area while TSS is total suspended sediment in mg/L, and the estimated value is conveniently reported on $t\ km^{-2}y^{-1}$. This approach allows for a comprehensive understanding of how physical and chemical weathering processes contribute to landscape evolution in the basin. The discharge-weighted PWR provides insights into seasonal variations in erosion and helps identify how different climatic and hydrological factors drive these processes³⁵. The relationship between SWR and PWR is crucial for understanding the balance between the chemical dissolution of minerals and the mechanical breakdown of rocks, further illuminating the complex interactions within the weathering system of KVRB.

The PWR of KVRB is estimated on a seasonal basis, with a yearly discharge-weighted average used to assess the PWR and analyze its relationship with the SWR. For KRB, the PWR values during the PRE, MON, and POM are calculated as $5.76\ t\ km^{-2}\ y^{-1}$, $128.76\ t\ km^{-2}\ y^{-1}$, and $23.85\ t\ km^{-2}\ y^{-1}$ respectively, with a yearly weighted average of $84.5\ t\ km^{-2}\ y^{-1}$ at the outlet. In contrast, the PWR for VRB during the same periods is $2.01\ t\ km^{-2}\ y^{-1}$, $27.24\ t\ km^{-2}\ y^{-1}$, and $2.65\ t\ km^{-2}\ y^{-1}$ respectively, yielding a yearly weighted average of $18.07\ t\ km^{-2}\ y^{-1}$ at the outlet. The higher annual average of PWR in KRB is attributed to the higher PWR values in the MON season for KRB. This is due to the higher discharge rate and corresponding higher TSS during monsoon season, which signify that the physical weathering plays a significant role in MON season for KRB. The lower PRE and POM values of KRB suggest that solute weathering plays a more dominant role than physical weathering during both seasons. But in VRB, the annual PWR values are lower compared to the SWR signifies the pronounced role of SWR over PWR. This contraction of both rivers in PWR estimation is due to the steep and gentler topographical gradient prevailing in the KRB and VRB respectively.

Summary and Conclusions

The tropical mountainous rivers, Karman River Basin (KRB) and Vamanapuram River Basin (VRB), together referred to as KVRB, flowing through the Southern Granulite Terrain (SGT) are studied for understanding the dissolved load sources, controlling mechanisms, source-wise solute load, silicate weathering rates, and CO_2

consumption rates. The dominant controlling mechanism of the dissolved solute load for KVRB is identified as silicate weathering, followed by atmospheric and anthropogenic input. The chemical mass balance model quantifies the contribution from each source and confirms that the silicate weathering is contributing more i.e., 50.44% and 64.41% for KRB and VRB respectively, while the anthropogenic and atmospheric inputs are 34.60% and 19.73% respectively at the outlet. This finding further evaluates the SWR and CCR of the basins. The estimated SWR is higher in KRB ($30.96 \text{ t km}^{-2} \text{ yr}^{-1}$) compared to VRB ($22.89 \text{ t km}^{-2} \text{ yr}^{-1}$) and the CCR is too high in KRB ($1.16 \times 10^6 \text{ mole km}^{-2} \text{ yr}^{-1}$) compared to the latter ($3.20 \times 10^5 \text{ mole km}^{-2} \text{ yr}^{-1}$). This suggests that the KVRB is experiencing comparable rates of silicate weathering compared to the Gurupur ($38 \text{ t km}^{-2} \text{ yr}^{-1}$), Muvatupuzha ($27 \text{ t km}^{-2} \text{ yr}^{-1}$), Chandragiri–Payaswini ($39 \text{ t km}^{-2} \text{ yr}^{-1}$), Sharavati ($27 \text{ t km}^{-2} \text{ yr}^{-1}$), Gad ($40 \text{ t km}^{-2} \text{ yr}^{-1}$), Tapti ($33.6 \text{ t km}^{-2} \text{ yr}^{-1}$), Godavari ($34.69 \text{ t km}^{-2} \text{ yr}^{-1}$), Narmada ($33.9 \text{ t km}^{-2} \text{ yr}^{-1}$) and Swarnamukhi ($30.57 \text{ t km}^{-2} \text{ yr}^{-1}$). Moreover, they are higher than some of the largest river basins such as Amazon ($13 \text{ t km}^{-2} \text{ yr}^{-1}$), Mississippi ($3.8 \text{ t km}^{-2} \text{ yr}^{-1}$), Yangtze ($5.5 \text{ t km}^{-2} \text{ yr}^{-1}$), Mackenzie ($1.8 \text{ t km}^{-2} \text{ yr}^{-1}$), Congo ($4.3 \text{ t km}^{-2} \text{ yr}^{-1}$), and Nile ($0.8 \text{ t km}^{-2} \text{ yr}^{-1}$). This higher silicate weathering rates of KVRB is due to the granulite terrain with steep slopes, high rainfall, high temperatures and humid nature compared to other regions. Further, these higher values of SWR and CCR are attributed to the estimating method utilized compared with other studies as this study used rock ratios of the existing lithology of the basin rather using the world average rock ratios used by others. Moreover, it is also observed that the granulite rocks of KRB are more susceptible to erosion and weathering; this also validates the higher silicate weathering in the basin in all seasons though their contribution varies due to climatic effects. Moreover, the Arrhenius plot shows that the temperature is an important component in controlling the silicate weathering. The moderate correlation of Si with temperature ($R^2 \approx 0.57$) signifies that rather than higher temperature fluctuations and associated humid nature favors the SWR rates of both basins. The higher rates of silicate weathering are also confirmed with the estimation of activation energy for the KVRB which is $\sim 25 \text{ kJ mol}^{-1}$, which signifies the lower silicate weathering activation. Moreover, the physical weathering rates (PWR) estimation shows that the KRB experiences more PWR than VRB specifically in the MON season. These findings conclude that silicate weathering is an important dissolved solute load-deriving mechanism as it contributes more to KVRB. Compared with other rivers of WG's, KRB shows a higher SWR rate and VRB shows less. This study highlights the significant role of silicate weathering and CO₂ consumption in the regional carbon budget of the Karamana and Vamanapuram River Basins. The high weathering rates in KRB, in particular, suggest that these processes contribute to local carbon sequestration, potentially offsetting carbon emissions in the region. On a global scale, the study shows that tropical mountainous regions with high weathering rates could play a more substantial role in the global carbon cycle than previously recognized. These findings emphasize the importance of considering regional weathering processes in global carbon models to better understand carbon sequestration dynamics.

Data availability

The authors confirm that all data generated or analyzed during this study are included in this manuscript's Table 1. Any additional information regarding the calculation part will be provided upon reasonable request from the corresponding author.

Received: 21 October 2024; Accepted: 17 February 2025

Published online: 05 April 2025

References

- Zhu, C. & Schwartz, F. W. Hydrogeochemical processes and controls on water quality and water management. *Elements* **7** (3), 169–174 (2011).
- Kajita, H. et al. Seasonal and Spatial variations of chemical weathering in the Mekong basin: from the headwaters to the lower reaches. *Aquat. Geochem.* **26**, 137–159 (2020).
- Gupta, H., Chakrapani, G. J., Selvaraj, K. & Kao, S. J. The fluvial geochemistry, contributions of silicate, carbonate and saline-alkaline components to chemical weathering flux and controlling parameters: Narmada river (Deccan Traps), India. *Geochim. Cosmochim. Acta.* **75** (3), 800–824 (2011).
- Patel, P., Raju, N. J., Subramanian, V., Gossel, W. & Wycisk, P. Chemical weathering and atmospheric CO₂ consumption in the semi-arid Swarnamukhi basin (Peninsular India) estimated from river water geochemistry. *Appl. Geochem.* **113**, 104520 (2020).
- Gaillardet, J., Dupré, B. & Allègre, C. J. A global geochemical mass budget applied to the congo basin rivers: erosion rates and continental crust composition. *Geochim. Cosmochim. Acta.* **59** (17), 3469–3485 (1995).
- Millot, R., Gaillardet, J., Dupré, B. & Allègre, C. J. The global control of silicate weathering rates and the coupling with physical erosion: new insights from rivers of the Canadian shield. *Earth Planet. Sci. Lett.* **196** (1–2), 83–98 (2002).
- Krishnaswami, S. & Singh, S. K. Chemical weathering in the river basins of the Himalaya, India. *Curr. Sci.* **89**, 841–849 (2005).
- Xu, Z., Shi, C., Tang, Y. & Han, H. Chemical and strontium isotopic compositions of the Hanjiang basin rivers in China: anthropogenic impacts and chemical weathering. *Aquat. Geochem.* **17**, 243–264 (2011).
- Pattanaik, J. K., Balakrishnan, S., Bhutani, R. & Singh, P. Estimation of weathering rates and CO₂ drawdown based on solute load: significance of granulites and gneisses dominated weathering in the Kaveri river basin, Southern India. *Geochim. Cosmochim. Acta.* **121**, 611–636 (2013).
- Herath, I. K., Wu, S. J., Ma, M. H., Jianli, W. & Chandrajith, R. Tracing controlling factors of riverine chemistry in a headwater tributary of the Yangtze river, China, inferred from geochemical and stable isotopic signatures. *Environ. Sci. Pollut. Res.* **26**, 23899–23922 (2019).
- Gislason, S. R. & Oelkers, E. H. *Silicate Rock Weathering and the Global Carbon Cycle* 84–103 (Contribution of Geochemistry to the Study of the Earth, 2011).
- Deepthy, R. & Balakrishnan, S. Climatic control on clay mineral formation: evidence from weathering profiles developed on either side of the Western Ghats. *J. Earth Syst. Sci.* **114**, 545–556 (2005).
- Kasting, J. F. The goldilocks planet? How silicate weathering maintains Earth just right. *Elements: Int. Magazine Mineralogy Geochem. Petrol.* **15** (4), 235–240 (2019).
- Jha, P. K., Tiwari, J., Singh, U. K., Kumar, M. & Subramanian, V. Chemical weathering and associated CO₂ consumption in the Godavari river basin, India. *Chem. Geol.* **264** (1–4), 364–374 (2009).

15. Bastia, F. & Equeenuddin, S. M. Chemical weathering and associated CO₂ consumption in the Mahanadi river basin, India. *J. Asian Earth Sci.* **174**, 218–231 (2019).
16. RamyaPriya, R. & Elango, L. Atmospheric CO₂ consumption by rock weathering over a five year period in a large non-perennial tropical river basin of Southern India. *Environ. Sci. Pollut. Res.* **28**, 26461–26478 (2021).
17. Drever, J. I. & Zobrist, J. Chemical weathering of silicate rocks as a function of elevation in the Southern Swiss alps. *Geochim. Cosmochim. Acta.* **56** (8), 3209–3216 (1992).
18. Stallard, R. F. Relating chemical and physical erosion. *Rev. Mineral. Geochem.* **31** (1), 543–564 (1995).
19. Bluth, G. J. & Kump, L. R. Lithologic and climatologic controls of river chemistry. *Geochim. Cosmochim. Acta.* **58** (10), 2341–2359 (1994).
20. Galy, A. & France-Lanord, C. Weathering processes in the Ganges–Brahmaputra basin and the riverine alkalinity budget. *Chem. Geol.* **159** (1–4), 31–60 (1999).
21. Blum, J. D., Gazis, C. A., Jacobson, A. D., Chamberlain, P. & C. Carbonate versus silicate weathering in the Raikhot watershed within the high Himalayan crystalline series. *Geology* **26** (5), 411–414 (1998).
22. Berner, R. A. Weathering, plants, and the long-term carbon cycle. *Geochim. Cosmochim. Acta.* **56** (8), 3225–3231 (1992).
23. White, A. F. & Blum, A. E. Effects of climate on chemical weathering in watersheds. *Geochim. Cosmochim. Acta.* **59** (9), 1729–1747 (1995).
24. Gaillardet, J., Dupré, B., Louvat, P. & Allegre, C. J. Global silicate weathering and CO₂ consumption rates deduced from the chemistry of large rivers. *Chem. Geol.* **159** (1–4), 3–30 (1999).
25. Gaillardet, J. et al. Orography-driven chemical denudation in the lesser Antilles: evidence for a new feed-back mechanism stabilizing atmospheric CO₂. *Am. J. Sci.* **311** (10), 851–894 (2011).
26. Gurumurthy, G. P. et al. Controls on intense silicate weathering in a tropical river, Southwestern India. *Chem. Geol.* **300**, 61–69 (2012).
27. Velbel, M. A. & Price, J. R. Solute geochemical mass-balances and mineral weathering rates in small watersheds: methodology, recent advances, and future directions. *Appl. Geochem.* **22** (8), 1682–1700 (2007).
28. Lyons, W. B., Carey, A. E., Hicks, D. M. & Nezat, C. A. Chemical weathering in high-sediment-yielding watersheds, New Zealand. *J. Geophys. Research: Earth Surf.* **110**, F1 (2005).
29. Jacobson, A. D., Blum, J. D., Chamberlain, C. P., Craw, D. & Koons, P. O. Climatic and tectonic controls on chemical weathering in the New Zealand Southern alps. *Geochim. Cosmochim. Acta.* **67** (1), 29–46 (2003).
30. West, A. J. Thickness of the chemical weathering zone and implications for erosional and climatic drivers of weathering and for carbon-cycle feedbacks. *Geology* **40** (9), 811–814 (2012).
31. Hartmann, J., Jansen, N., Dürr, H. H., Kempe, S. & Köhler, P. Global CO₂-consumption by chemical weathering: what is the contribution of highly active weathering regions? *Glob. Planet Change.* **69** (4), 185–194 (2009).
32. Raymo, M. E. & Ruddiman, W. F. Tectonic forcing of late Cenozoic climate. *Nature* **359** (6391), 117–122 (1992).
33. Krishnaswami, S. & Singh, S. K. Silicate and carbonate weathering in the drainage basins of the Ganga-Ghaghara-Indus head waters: contributions to major ion and Sr isotope geochemistry. *Proc. Indian Acad. Sciences-Earth Planet. Sci.* **107**, 283–291 (1998).
34. Probst, J. L., Mortatti, J. & Tardy, Y. Carbon river fluxes and weathering CO₂ consumption in the Congo and Amazon river basins. *Appl. Geochem.* **9** (1), 1–13 (1994).
35. Boeglin, J. L. & Probst, J. L. Physical and chemical weathering rates and CO₂ consumption in a tropical lateritic environment: the upper Niger basin. *Chem. Geol.* **148** (3–4), 137–156 (1998).
36. Li, S., Lu, X. X. & Bush, R. T. Chemical weathering and CO₂ consumption in the lower Mekong river. *Sci. Total Environ.* **472**, 162–177 (2014).
37. Zhang, S. R. et al. Water chemistry of the Zhujiang (Pearl River): natural processes and anthropogenic influences. *J. Geophys. Research: Earth Surf.* **112**, F01011 (2007).
38. Gao, Q. et al. Chemical weathering and CO₂ consumption in the Xijiang river basin, South China. *Geomorphology* **106** (3–4), 324–332 (2009).
39. Wu, L., Huh, Y., Qin, J., Du, G. & van Der Lee, S. Chemical weathering in the upper Huang he (Yellow River) draining the Eastern Qinghai-Tibet plateau. *Geochim. Cosmochim. Acta.* **69** (22), 5279–5294 (2005).
40. Wu, W., Xu, S., Yang, J. & Yin, H. Silicate weathering and CO₂ consumption deduced from the seven Chinese rivers originating in the Qinghai-Tibet plateau. *Chem. Geol.* **249** (3–4), 307–320 (2008).
41. Chen, J., Wang, F., Xia, X. & Zhang, L. Major element chemistry of the Changjiang (Yangtze River). *Chem. Geol.* **187** (3–4), 231–255 (2002).
42. Chetelat, B. et al. Geochemistry of the dissolved load of the Changjiang basin rivers: anthropogenic impacts and chemical weathering. *Geochim. Cosmochim. Acta.* **72** (17), 4254–4277 (2008).
43. Han, G. & Liu, C. Q. Water geochemistry controlled by carbonate dissolution: a study of the river waters draining karst-dominated terrain, Guizhou Province, China. *Chem. Geol.* **204** (1–2), 1–21 (2004).
44. Ramesh, R. & Subramanian, V. Nature of the dissolved load of the Krishna river basin, India. *J. Hydrol.* **103** (1–2), 139–155 (1988).
45. Singh, O., Sharma, M. C., Sarangi, A. & Singh, P. Spatial and Temporal variability of sediment and dissolved loads from two alpine watersheds of the lesser Himalayas. *Catena* **76** (1), 27–35 (2008).
46. Panda, D. K., Kumar, A. & Mohanty, S. Recent trends in sediment load of the tropical (Peninsular) river basins of India. *Glob. Planet Change.* **75** (3–4), 108–118 (2011).
47. Yadav, S. K. & Chakrapani, G. J. Geochemistry dissolved elemental flux rates, and dissolution kinetics of lithologies of Alaknanda and Bhagirathi rivers in Himalayas, India. *Environ. Earth Sci.* **62**, 593–610 (2011).
48. Lupker, M., France-Lanord, C., Galy, V., Lavé, J. & Kudrass, H. Increasing chemical weathering in the Himalayan system since the last glacial maximum. *Earth Planet. Sci. Lett.* **365**, 243–252 (2013).
49. Singh, V. B., Ramanathan, A. L., Pottakkal, J. G. & Kumar, M. Seasonal variation of the solute and suspended sediment load in Gangotri glacier meltwater, central Himalaya, India. *J. Asian Earth Sci.* **79**, 224–234 (2014).
50. Maharana, C., Gautam, S. K., Singh, A. K. & Tripathi, J. K. Major ion chemistry of the son river, India: weathering processes, dissolved fluxes and water quality assessment. *J. Earth Syst. Sci.* **124**, 1293–1309 (2015).
51. Sarath, P. K. et al. Seasonal, weathering and water use controls of silicon cycling along the river flow in two contrasting basins of South India. *Chem. Geol.* **604**, 120883 (2022).
52. Dalai, T. K., Krishnaswami, S. & Sarin, M. M. Major ion chemistry in the headwaters of the Yamuna river system: chemical weathering, its temperature dependence and CO₂ consumption in the Himalaya. *Geochim. Cosmochim. Acta.* **66** (19), 3397–3416 (2002).
53. Quade, J., English, N. & DeCelles, P. G. Silicate versus carbonate weathering in the Himalaya: a comparison of the Arun and Seti river watersheds. *Chem. Geol.* **202** (3–4), 275–296 (2003).
54. Chakrapani, G. J., Saini, R. K. & Yadav, S. K. Chemical weathering rates in the Alaknanda–Bhagirathi river basins in Himalayas, India. *J. Asian Earth Sci.* **34** (3), 347–362 (2009).
55. Milliman, J. D. & Farnsworth, K. L. *River Discharge To the Coastal Ocean: a Global Synthesis* (Cambridge University Press, 2013).
56. Padmalal, D. et al. Water quality and dissolved inorganic fluxes of N, P, SO₄, and K of a small catchment river in the Southwestern Coast of India. *Environ. Monit. Assess.* **184** (3), 1541–1557 (2012).

57. Reddy, S. K. K., Gupta, H., Reddy, D. V. & Kumar, D. *The Suitability of Surface Waters from Small west-flowing Rivers for Drinking, Irrigation, and Aquatic Life from a Global Biodiversity Hotspot (Western Ghats, India)* 2838613–38628 (Environmental Science and Pollution Research, 2021).
58. Tripti, M., Gurumurthy, G. P., Lambs, L., Riotte, J. & Balakrishna, K. Water and organic carbon cycles in monsoon-driven humid tropics of the Western Ghats mountain belt, India: insights from stable isotope approach. *J. Geol. Soc. India*. **92**, 579–587 (2018).
59. Prasad, M. B. K. & Ramanathan, A. L. Solute sources and processes in the Achankovil river basin, Western Ghats, Southern India/ Sources de solutés et processus associés Dans Le Bassin du fleuve Achankovil, Ghats Occidentaux, inde du Sud. *Hydrol. Sci. J.* **50**(2), 341–354 (2005).
60. Thomas, J., Joseph, S. & Thrivikramji, K. P. Discriminant analysis for characterization of hydrochemistry of two mountain river basins of contrasting climates in the Southern Western Ghats, India. *Environ. Monit. Assess.* **187**, 1–21 (2015a).
61. Thomas, J., Joseph, S. & Thrivikramji, K. P. Hydrochemical variations of a tropical mountain river system in a rain shadow region of the Southern Western Ghats, Kerala, India. *Appl. Geochem.* **63**, 456–471 (2015b).
62. Nisha, B. K., Balakrishna, K., Udayashankar, H. N. & Manjunatha, B. R. Chemical weathering and carbon dioxide consumption in a small tropical river catchment, Southwestern India. *Aquat. Geochem.* **27** (3), 173–206 (2021).
63. Amrith, V. N., Arun, K., Balakrishna, K., Udayashankar, H. N. & Khare, N. Major ion chemistry and silicate weathering rate of a small Western Ghats river, Sharavati, Southwestern India. *Appl. Geochem.* **136**, 105182 (2022).
64. Arun, K. et al. Chemical denudation in a small mountainous coastal river in the tropics: insights from Kali river, Southwestern India. *Appl. Geochem.* **137**, 105198 (2022).
65. Vijith, H., Prasannakumar, V., Pratheesh, P., Krishnan, M. N. & Mohan, M. S. Evaluation of geomorphic expressions of bedrock channels in the Western Ghats of Southern Kerala, India, through quantitative analysis. *Arab. J. Geosci.* **9**, 1–15 (2016).
66. Padmanabhan, N. HISTORY OF KERALA I. NEW WRITING, 164, 194. (2013).
67. Harikumar, P. S. WATER QUALITY STATUS OF THIRUVANATHAPURAM DISTRICT, KERALA. 1–4. (2017).
68. Uppendra, B. et al. Mechanisms controlling the dissolved load, chemical weathering and CO₂ consumption rates of cauvery river, South India: role of secondary soil minerals. *Environ. Earth Sci.* **81** (3), 103 (2022).
69. Syvitski, J. P. M. & Milliman, J. D. Geology, geography, and humans battle for dominance over the delivery of fluvial sediment to the coastal ocean. *J. Geol.* **115** (1), 1–19 (2007).
70. Horowitz, A. J. Determining annual suspended sediment and sediment-associated trace element and nutrient fluxes. *Sci. Total Environ.* **400** (1–3), 315–343 (2008).
71. Ding, H. et al. Geochemistry of the dissolved loads of the Liao river basin in Northeast China under anthropogenic pressure: chemical weathering and controlling factors. *J. Asian Earth Sci.* **138**, 657–671 (2017).
72. Sarin, M. M., Krishnaswami, S., Dilli, K., Somayajulu, B. L. K. & Moore, W. S. Major ion chemistry of the Ganga-Brahmaputra river system: weathering processes and fluxes to the Bay of Bengal. *Geochim. Cosmochim. Acta.* **53** (5), 997–1009 (1989).
73. Négrel, P., Allègre, C. J., Dupré, B. & Lewin, E. Erosion sources determined by inversion of major and trace element ratios and strontium isotopic ratios in river water: the congo basin case. *Earth Planet. Sci. Lett.* **120** (1–2), 59–76 (1993).
74. Grosbois, C., Négrel, P., Fouillac, C. & Grimaud, D. Dissolved load of the Loire river: chemical and isotopic characterization. *Chem. Geol.* **170** (1–4), 179–201 (2000).
75. Xu, Z. & Liu, C. Q. Chemical weathering in the upper reaches of Xijiang river draining the Yunnan–Guizhou plateau, Southwest China. *Chem. Geol.* **239** (1–2), 83–95 (2007).
76. Zhang, Q., Jin, Z., Zhang, F. & Xiao, J. Seasonal variation in river water chemistry of the middle reaches of the yellow river and its controlling factors. *J. Geochem. Explor.* **156**, 101–113 (2015).
77. Rao, P. P., Momin, G. A., Safai, P. D., Pillai, A. G. & Khemani, L. T. Rain water and throughfall chemistry in the silent Valley forest in South India. *Atmos. Environ.* **29** (16), 2025–2029 (1995).
78. Krishnakumar, A., Das, R. & Puthalath, S. *Assessment of the Quality of Water Resources in Coastal Urban Lands of Two Small Catchment Rivers, Southwest India* (An International Journal, 2017).
79. Das, A., Krishnaswami, S., Sarin, M. M. & Pande, K. Chemical weathering in the Krishna basin and Western Ghats of the Deccan traps, India: rates of basalt weathering and their controls. *Geochim. Cosmochim. Acta.* **69** (8), 2067–2084 (2005).
80. Knoll, M. A. & James, W. C. Effect of the advent and diversification of vascular land plants on mineral weathering through geologic time. *Geology* **15** (12), 1099–1102 (1987).
81. Berner, R. A. GEOCARB II: A revised model of atmospheric CO₂ over phanerozoic time. *Am. J. Science; (United States)* **294**(1), 56–91 (1994).
82. Walker, J. C., Hays, P. B. & Kasting, J. F. A negative feedback mechanism for the long-term stabilization of Earth's surface temperature. *J. Geophys. Research: Oceans.* **86** (C10), 9776–9782 (1981).
83. Raymo, M. E. Geochemical evidence supporting TC Chamberlin's theory of glaciation. *Geology* **19** (4), 344–347 (1991).
84. Viers, J. et al. Evidence of Zn isotopic fractionation in a soil–plant system of a pristine tropical watershed (Nsimi, Cameroon). *Chem. Geol.* **239** (1–2), 124–137 (2007).
85. West, A. J., Galy, A. & Bickle, M. Tectonic and Climatic controls on silicate weathering. *Earth Planet. Sci. Lett.* **235** (1–2), 211–228 (2005).
86. Thomas, J., Joseph, S., Thrivikramji, K. P., Manjusree, T. M. & Arunkumar, K. S. Seasonal variation in major ion chemistry of a tropical mountain river, the southern Western Ghats, Kerala, India. *Environmental earth sciences*, 71, 2333–2351. (2014).
87. Mortatti, J. & Probst, J. L. Silicate rock weathering and atmospheric/soil CO₂ uptake in the Amazon basin estimated from river water geochemistry: seasonal and spatial variations. *Chem. Geol.* **197** (1–4), 177–196 (2003).
88. Laraque, A. et al. Seasonal variability of total dissolved fluxes and origin of major dissolved elements within a large tropical river: the Orinoco, Venezuela. *J. S. Am. Earth Sci.* **44**, 4–17. <https://doi.org/10.1016/j.jsames.2012.12.011> (2013).
89. Rangasamy, E. & Muniyandi, M. Current status of stream water quality around selected tea gardens from Southern Western Ghats, Tamil Nadu, India–A case study. *HydroResearch* **7**, 99–108 (2024).
90. Sundaray, S. K., Panda, U. C., Nayak, B. B. & Bhatta, D. Multivariate statistical techniques for the evaluation of Spatial and Temporal variations in water quality of the Mahanadi river–estuarine system (India)–a case study. *Environ. Geochem. Health.* **28**, 317–330 (2006).
91. Rahman, M. A. & Huda, M. E. Study of the seasonal variations in physicochemical and biological aspects of the Padma river at Paturia Ghat, Manikganj. *Jahangirnagar Univ. Environ. Bull.* **1**, 55–66 (2012).
92. Rani, N., Sinha, R. K., Prasad, K. & Kedia, D. K. Assessment of Temporal variation in water quality of some important rivers in middle gangetic plains, India. *Environ. Monit. Assess.* **174**, 401–415 (2011).
93. Maity, S., Maiti, R. & Senapati, T. Evaluation of spatio-temporal variation of water quality and source identification of conducive parameters in Damodar river, India. *Environ. Monit. Assess.* **194** (4), 308 (2022).
94. Das, B. K., Boruah, P. & Kar, D. Study of seasonal variation of water quality of river Siang in Arunachal Pradesh, India. *IOSR J. Environ. Sci. Toxicol. Food Technol. (IOSR-JESTFT)*. **8** (2IV), 11–20 (2014).
95. Maitra, A., Chatterjee, A., Keesari, T. & Gupta, S. Forming topography in granulite terrains: evaluating the role of chemical weathering. *J. Earth Syst. Sci.* **129**, 1–13 (2020).
96. Ajaykrishnan, K., Santhosh, S. & Sobha, V. A Spatial model for water resource management in Karamana river basin using geoinformatics. *Int. J. Eng. Innovat Technol. (IJEIT)*. **4** (4), 194–199 (2014).
97. Trivikramaji, K. P. & Joseph, S. Solute variation in some minorsheds, Kerala, India. In Proceedings. Workshop on Ecohydrology. Sch of Environ. Science., Jawaharlal Nehru University, New Delhi (pp. 295–304). (2001).

98. Sharma, S. K. & Subramanian, V. Hydrochemistry of the Narmada and Tapi rivers, India. *Hydrol. Processes: Int. J.* **22** (17), 3444–3455 (2008).
99. Moon, S., Huh, Y., Qin, J. & van Pho, N. Chemical weathering in the Hong (Red) river basin: rates of silicate weathering and their controlling factors. *Geochim. Cosmochim. Acta.* **71** (6), 1411–1430 (2007).
100. Fernandes, A. M., da Conceição, F. T., Junior, E. P. S., de Souza Sardinha, D. & Mortatti, J. Chemical weathering rates and atmospheric/soil CO₂ consumption of igneous and metamorphic rocks under tropical climate in southeastern Brazil. *Chem. Geol.* **443**, 54–66 (2016).
101. Brady, P. V. The effect of silicate weathering on global temperature and atmospheric CO₂. *J. Geophys. Research: Solid Earth.* **96** (B11), 18101–18106 (1991).
102. Dessert, C. et al. Erosion of Deccan traps determined by river geochemistry: impact on the global climate and the ⁸⁷Sr/⁸⁶Sr ratio of seawater. *Earth Planet. Sci. Lett.* **188**, 459–474 (2001).
103. White, A. F. & Brantley, S. L. Chemical weathering rates of silicate minerals. In M. J. (Ed.), *Geochemistry of the Earth's Surface* (pp. 259–277). (2003).
104. Li, S., Xu, Z., Wang, H., Wang, J. & Zhang, Q. Geochemistry of the upper Han river basin, China: 3: anthropogenic inputs and chemical weathering to the dissolved load. *Chem. Geol.* **264** (1–4), 89–95 (2009).
105. Fan, B. L. et al. Characteristics of carbonate, evaporite and silicate weathering in Huanghe river basin: A comparison among the upstream, midstream and downstream. *J. Asian Earth Sci.* **96**, 17–26 (2014).
106. Sun, H., Han, J., Li, D., Zhang, S. & Lu, X. Chemical weathering inferred from riverine water chemistry in the lower Xijiang basin, South China. *Sci. Total Environ.* **408** (20), 4749–4760 (2010).
107. Shanmugasundharam, A., Akhina, S. N., Adhithya, R. P., Singh, D. S. H. & Krishnakumar, S. Water quality index (WQI), multivariate statistical and GIS for assessment of surface water quality of Karamana river estuary, West Coast of India. *Total Environ. Res. Themes.* **6**, 100031 (2023).
108. Kumar, R. et al. Chemometric approach to evaluate the chemical behavior of rainwater at high altitude in Shaune Garang catchment, Western Himalaya. *Sci. Rep.* **12**, 12774. <https://doi.org/10.1038/s41598-022-15422-0> (2022).
109. Kumar, R. et al. Hydro-geochemical characteristics of glacial meltwater from Naradu glacier catchment, Western Himalaya. *Environ. Earth Sci.* **78**, 683. <https://doi.org/10.1007/s12665-019-8687-0> (2019).

Acknowledgements

The authors sincerely thank the Director, NCESS, and the Biogeochemistry group head, NCESS for their valuable support. The authors also convey gratitude towards the Solid Earth Research Group (SERG), NCESS, for providing analytical facilities.

Author contributions

B.U. and M.C. wrote the main manuscript and prepared the Maps, Figs. 1, 2, 3, 4, 5, 6 and 7, and Tables 1, 2, 3 and 4. The S.R., G.S., S.K.R., K.A.K. and V.A. contributed to fieldwork and analysis as well as reviewed the manuscript.

Funding

The authors did not receive support from any organization for the submitted work.

Declarations

Competing interests

The authors declare no competing interests.

Ethics approval

“All authors have read, understood, and have complied as applicable with the statement on “Ethical responsibilities of Authors” as found in the instructions for authors and are aware that with minor exceptions, no changes can be made to authorship once the paper is submitted.”

Additional information

Supplementary Information The online version contains supplementary material available at <https://doi.org/10.1038/s41598-025-90913-4>.

Correspondence and requests for materials should be addressed to B.U.

Reprints and permissions information is available at www.nature.com/reprints.

Publisher's note Springer Nature remains neutral with regard to jurisdictional claims in published maps and institutional affiliations.

Open Access This article is licensed under a Creative Commons Attribution-NonCommercial-NoDerivatives 4.0 International License, which permits any non-commercial use, sharing, distribution and reproduction in any medium or format, as long as you give appropriate credit to the original author(s) and the source, provide a link to the Creative Commons licence, and indicate if you modified the licensed material. You do not have permission under this licence to share adapted material derived from this article or parts of it. The images or other third party material in this article are included in the article's Creative Commons licence, unless indicated otherwise in a credit line to the material. If material is not included in the article's Creative Commons licence and your intended use is not permitted by statutory regulation or exceeds the permitted use, you will need to obtain permission directly from the copyright holder. To view a copy of this licence, visit <http://creativecommons.org/licenses/by-nc-nd/4.0/>.

© The Author(s) 2025